AD-A159 531 LASER REMOTE SENSING OF ATMOSPHERIC POLLUTANTS(U) 1/1
MASSACHUSETTS INST OF TECH LEXINGTON LINCOLN LAB
D K KILLINGER ET AL. 30 SEP 84 ESD-TR-85-212
UNCLASSIFIED F19628-85-C-0002 F/G 13/2 NL

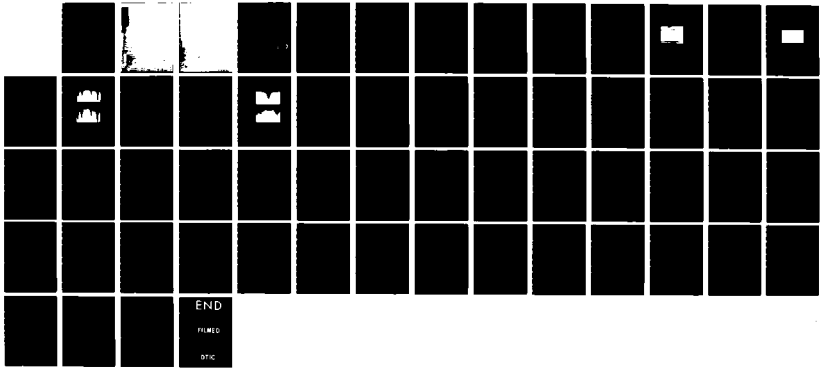

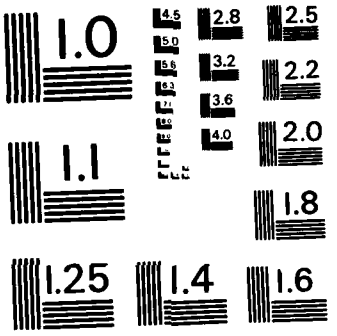

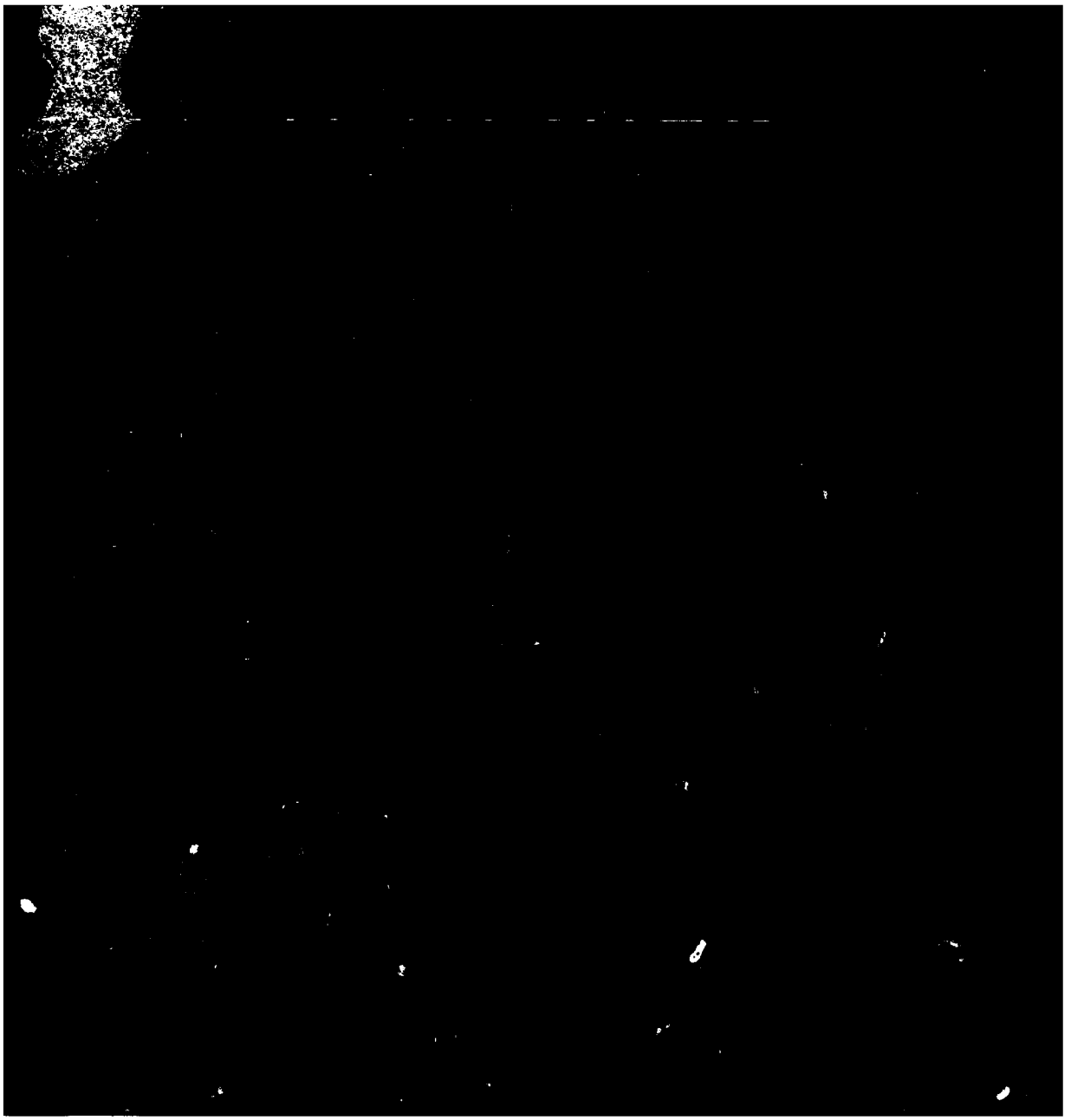

MASSACHUSETTS INSTITUTE OF TECHNOLOGY
LINCOLN LABORATORY

LASER REMOTE SENSING OF ATMOSPHERIC POLLUTANTS

D.K. KILLINGER
N. MENYUK
A. MOORADIAN

Group 82

FINAL REPORT
TO THE
AIR FORCE ENGINEERING AND SERVICES CENTER

1 OCTOBER 1983 — 30 SEPTEMBER 1984

ISSUED 26 JULY 1985

LEXINGTON MASSACHUSETTS

Contents

I. INTRODUCTION

This is the FY84 final report on the program entitled "Laser Remote Sensing of Atmospheric Pollutants" supported by the Air Force Engineering and Services Center and the Air Force Aerospace Medical Division. The effort is part of a larger ongoing program at Lincoln Laboratory to develop laser remote sensing techniques for the detection of chemical species in the atmosphere.

The specific tasks which were conducted during FY84 for this research program consisted of the following:

(1) The continuation of the CO_2 DIAL measurement program,

(2) Further development of the Co:MgF_2 DIAL system,

(3) Initial investigation of the use of the Co:MgF_2 DIAL system for range resolved DIAL measurements of atmospheric species,

(4) Establishment of the sensitivity of the Co:MgF_2 DIAL system for the remote sensing of atmospheric HCl, and

(5) Initial investigation of frequency-shifting techniques for the Co:MgF_2 laser.

Each of these tasks are described in detail in the following sections. Supportive documentation is included in the appendices.

II. CO_2 DIAL INVESTIGATIONS

The study of the use of CO_2 differential-absorption LIDAR (DIAL) for the remote sensing of atmospheric pollutants was continued during FY84 and consisted of two investigations. The specifics of these two investigations are presented in Appendix A and Appendix B. A synopsis of the studies are presented below.

A. Error Reduction in Laser Remote Sensing: Combined Effects of Cross-Correlation and Signal Averaging

A theoretical analysis was made of the extent to which the accuracy of a DIAL measurement may be improved by using different signal processing techniques, in particular the combined effects of signal-averaging and temporal cross-correlation. In addition, experimental results involving signal returns from a diffusely reflecting target using a dual-CO_2 laser DIAL system with both heterodyne and direct detection were found to be in excellent agreement with the theoretical analysis (Appendix A).

The DIAL experiments measured the effectiveness of using the ratio of signal returns from a dual-laser system in conjunction with signal averaging in improving measurement accuracy. In general, significant improvement was obtained by first averaging the individual LIDAR signals and then taking the ratios of the averaged signals in order to deduce the differential-absorption value. This is in contrast to taking the ratio of each pulse-pair DIAL return and then averaging this ratio; such analysis can lead to a significant error due to the exaggerated effect of small fluctuations in calculating the ratio value.

The degree of improvement was found to be strongly dependent upon the relative values of the standard deviation (fluctuation level) and the temporal cross-correlation and autocorrelation of the LIDAR signals. However, in general, the accuracy of the DIAL measurements was of the order of 3 to 5% for direct detection of hard target returns and of the order of 5 to 15% for hetrodyne detection. It should be added that these results are primarily applicable to our 10-Hz PRF CO_2 DIAL system and should not be construed to

apply to a higher PRF system. It is anticipated that a higher PRF system could, in principle, obtain a better measurement accuracy.

B. CO_2 Laser Remote Sensing of Atmospheric Ammonia

The CO_2 DIAL system was used to study the feasibility of the laser remote sensing of atmospheric ammonia (Appendix B). This study encompassed the determination of the optimum CO_2 laser lines for the remote sensing of ammonia, the first demonstration of the detection of atmospheric ammonia using a CO_2 DIAL system, and the observation of an interplay of the concentration of water vapor and ammonia under ambient conditions.

With CO_2 LIDAR returns obtained from topographic targets at a range of 2.7 km, the experiments demonstrated the ability of the DIAL system to remotely sense the presence of NH_3 with a path-averaged detection sensitivity of 5 parts per billion (ppb) at this range. The concentration of atmospheric ammonia was observed to vary between a negligible amount (less than 5 ppb) to values as high as 20 ppb. In addition, an apparent negative correlation between the measured concentration of ammonia and the separately measured relative humidity was observed; this negative correlation may be due to the solubility of ammonia in water vapor aerosols in the atmosphere.

III. Co:MgF_2 LASER DIAL SYSTEM DEVELOPMENT

The Co:MgF_2 laser reported in the FY83 Final Report was modified in order to increase laser output energy and spectral tunability. In addition, the DIAL system was changed to provide for computer control of the laser wavelength and DIAL data acquisition. Some of the details of the laser system are presented in the FY83 Final Report. The specific technical modifications are described in the following section.

Figure 1 shows a schematic of the Co:MgF_2 DIAL system. This system is similar to the previous system with the following changes: (1) the solid, intracavity etalon is now 0.25 mm thick and coated for 20% reflectivity at 1.6 micrometers, (2) the output mirror (M2) was changed in reflectivity to 90% from 95% to reduce the internal circulating laser energy which had previously caused optical damage in mirror M1, (3) the triple-element birefrigent tuning filter (BTF) was angle tuned through use of a Burleigh "Inchworm" and computer controlled, and (4) a 60 cm diameter Cassegrain telescope was used instead of the off-axis paraboloid.

The output energy of the Co:MgF_2 laser was approximately 10 mJ at a PRF of 3 Hz, the spectral linewidth was 0.15 cm^{-1}, and the pulse length was approximately 0.5 microseconds. The actual laser energy transmitted into the atmosphere was estimated to be about 7 mJ per pulse.

The temporal characteristics of the output energy are shown in Fig. 2 which presents a photograph of the oscilloscope trace of the free running (not Q-switched) and Q-switched Co:MgF_2 laser output. The multi-spike output under free-running conditions is typical of relaxation oscillations in a solid-state laser under nonequilibrium pump conditions.

The laser energy was limited, under Q-switched conditions, to less than 15 mJ/pulse by the damage threshold of the back mirror (M1 in Fig. 1) of the laser cavity. It is anticipated that this threshold can be raised by an order of magnitude by changes in the laser cavity and laser pumping scheme; these changes are currently being made.

The wavelength of the laser was monitored by use of a 1-m grating spectrometer coupled to a scanning 64-element pyroelectric detector array

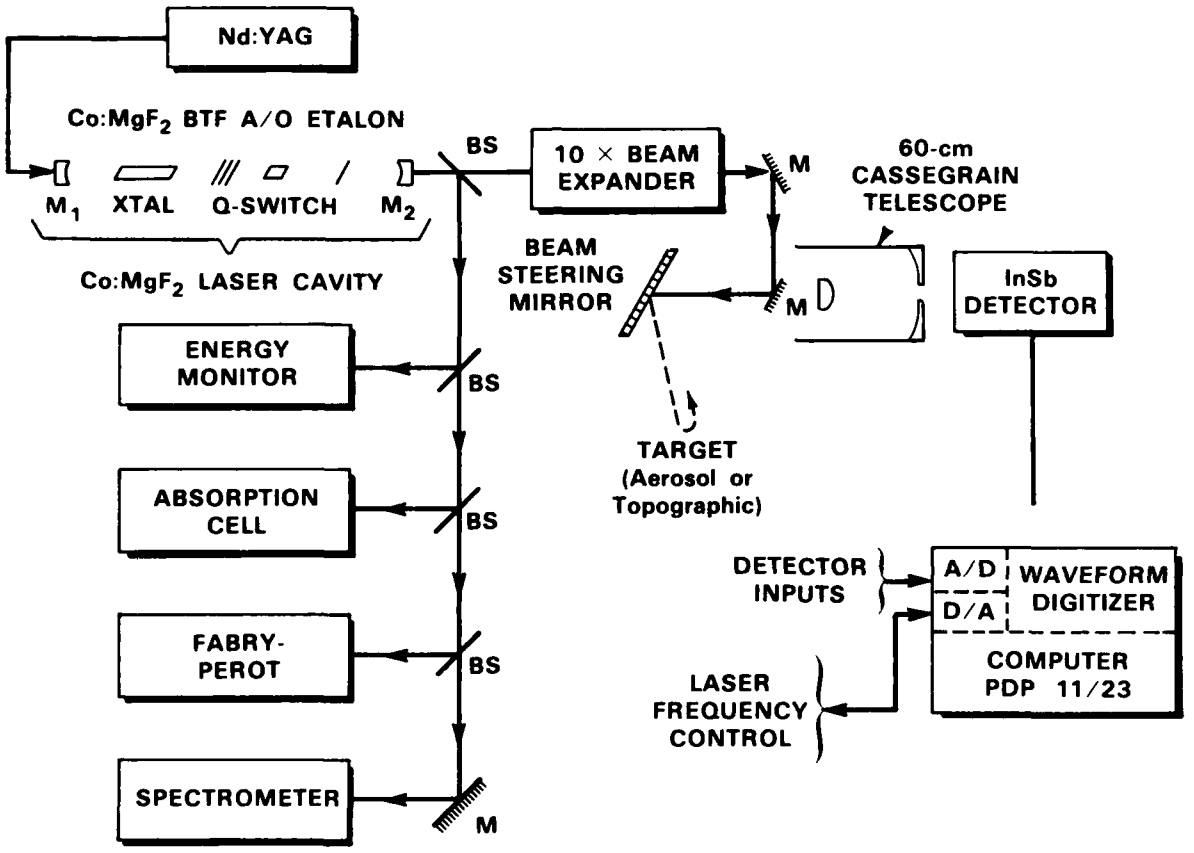

Figure 1. Schematic of $Co:MgF_2$ LIDAR system.

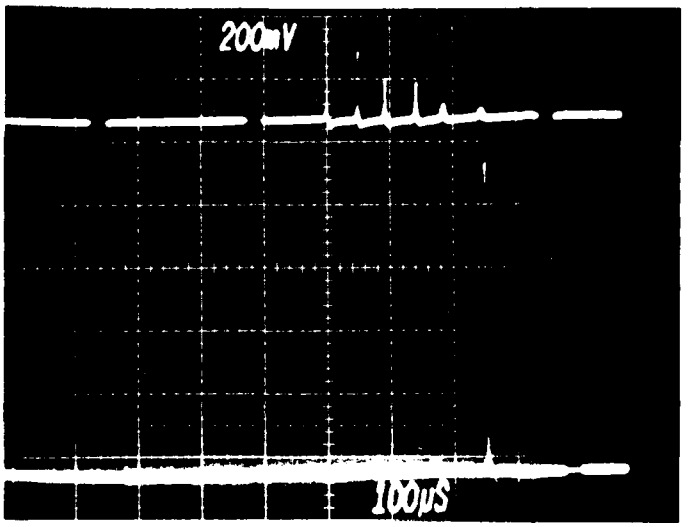

Figure 2. Oscilloscope trace of Co:MgF_2 laser pulse.

placed at the output focal plane of the spectrometer. The array provided for wavelength calibration of the laser on a single-shot basis with an accuracy of approximately 0.5 cm^{-1}. Figure 3 shows a photograph of the output of the spectral array detector . This system was used for coarse adjustment of the laser frequency and to ensure stable operation of the Co:MgF_2 laser. Finer spectral resolution was provided by a fixed, 0.5 cm spacing, air-gap Fabry-Perot etalon whose output was recorded by the computer as the laser frequency was scanned; this provided precise calibration of the wavelength of the laser as it was scanned.

In addition, a 1-m-long laboratory absorption cell was used for absorption calibration. The detected normalized absorption signal was collected by the computer system for comparison with the LIDAR (DIAL) absorption data.

The computer was used to control the wavelength of the Co:MgF_2 laser and to collect and analyze the LIDAR absorption cell, Fabry-Perot, and normalization (laser energy/pulse) signals. Two different computer programs were written which were used for path-averaged and range-resolved DIAL measurements.

For path-averaged measurements, the computer scanned the Co:MgF_2 laser in small increments over a 3 to 5 cm^{-1} frequency region and recorded the LIDAR and absorption cell data. The Fabry-Perot data was used to calibrate the wavelength position of the LIDAR and absorption cell data. For range-resolved data, the computer "toggled" the laser output between the two wavelengths chosen so that they were on-resonance and off-resonance to the absorption line of the DIAL detected species. The range-resolved LIDAR data was collected by a transient digitizer and averaged over a selected number of

NUMBER OF ARRAY ELEMENTS: 64
CENTER TO CENTER ARRAY SPACING: 100 μm

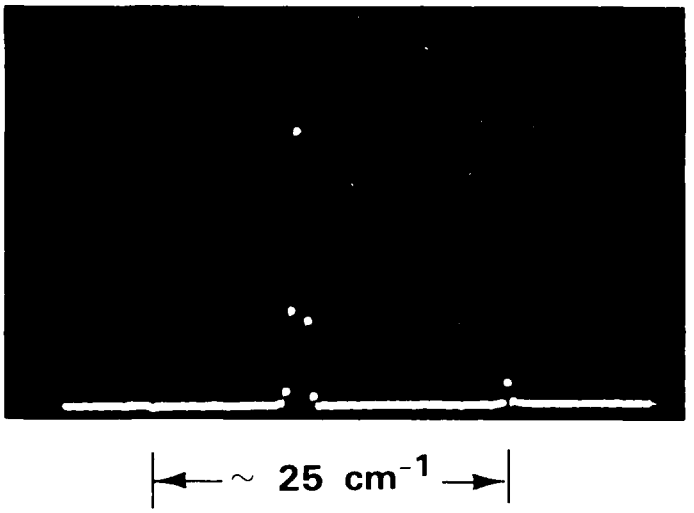

141549-N

Figure 3. Output of spectrometer pyroelectric array indicating spectral distribution of Co:MgF_2 laser pulse.

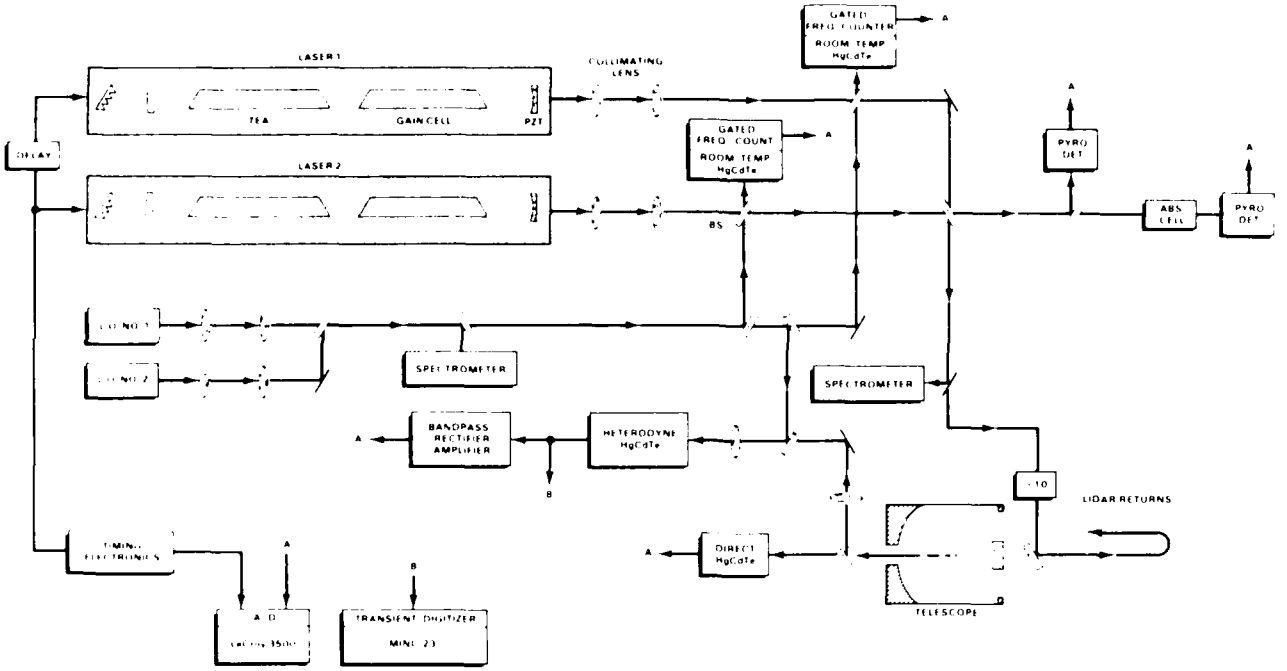

Fig. 1. Schematic of dual-CO_2 laser differential-absorption lidar system with capability of simultaneous heterodyne and direct detection of backscattered laser signals.

heterodyne and direct detection of the same backscattered lidar signals.

The DIAL system was used to measure and record the lidar returns from a diffusely reflecting target using both the direct- and heterodyne-detection systems. The target was located at a 2.7-km range from the laboratory. In each experiment, a total of 6144 normalized backscattered lidar signals from each laser was recorded for later statistical analysis. The process took 10 min, corresponding to a pulse repetition frequency (prf) of ~10 Hz.

A statistical analysis of the data was performed and included determination of the statistical parameters presented in the previous section. Specifically, the data were used to determine (1) the temporal autocorrelation coefficients, ρ_{x_1} and ρ_{x_2}, (2) the temporal cross correlation for pulse pairs ρ_c, for longer delays $\rho_{x_1x_2}$, and for the signal-averaged pairs ρ_{n_c}, (3) the variance of the individual lasers, $\sigma_{x_1}^2$ and $\sigma_{x_2}^2$, and (4) the variance of the mean, $\sigma_{n_{x_1}}^2$ and $\sigma_{n_{x_2}}^2$. From these parameters, $\sigma_{n\xi}^2$ was computed on the basis of Eqs. (5) and (8). In addition, after averaging the signals of each of the two lasers over n pulses, the ratio of these averages permitted a direct measurement of σ_{n_ξ}. Comparison of the computed and measured values of σ_{n_ξ} yielded a direct experimental determination of the limits of validity of Eqs. (3) and (5). The data also established the validity of Eq. (8) and, most important, permitted determination of the combined effectiveness of signal averaging and of the dual-laser capability in reducing measurement uncertainty under different experimental conditions. Details of the experimental results are given in the following section.

B. Experimental Results

In view of the different features of the experimental results obtained under various experimental conditions it was found convenient to divide the direct and heterodyne DIAL measurements into subgroups dependent on the relative numerical values of the standard deviation $\sigma_i (i = x,y)$ and the cross-correlation coefficient ρ_c. The subgroups discussed below include (1) small σ_i, small ρ_c; (2) large σ_i, large ρ_c; and (3) large σ_i, small ρ_c. This division was chosen because the different DIAL measurements indicate it is these relative values which determine the effect of signal averaging on the lidar returns. A fourth subgroup, namely, small σ_i and large ρ_c, is not considered because no experimental results obey these conditions; this is associated with the observation that uncorrelated noise often dominates lidar fluctuations at low σ_i levels, so that a large ρ_c value is incompatible with a small σ_i value.

1. *Small Standard Deviation and Small Cross Correlation*

Two distinct DIAL measurements involving the direct detection of backscattered lidar returns from a diffusely reflecting target had small σ_i and small ρ_c values. Under these experimental conditions, it was generally observed that σ_{x_1} and $\sigma_{x_2} \sim 0.2$ and that $\rho_c \sim 0.3$–0.4. However, while the experimental conditions were the same in the two experiments, the atmospheric conditions were different. In one of these experiments there was no distinctive variation in the average value of the returns over the 10-min experimental period. During the other experiment, there was a slow but al-

cross-correlation coefficient. This requires deriving the relationship between an effective signal-averaged temporal cross correlation ρ_{nc} and the individual pulse returns.

Equation (3) gives the approximate relationship between the uncertainty of the DIAL measurement σ_ξ with that of the individual laser return signals, σ_x and σ_y, and the pulse-pair cross correlation ρ_c. The terms in Eq. (3) refer to the full set or ensemble of data points which comprises the lidar return values. If one assumes that a total of Γ data points have been measured with each of the lasers, σ_x and σ_y represented the normalized standard deviations of the Γ data points from the respective lasers. Signal averaging over n signal returns, where $n \ll \Gamma$, then yields a new set of Γ/n data points, where each new data point is the average of n successive signal returns. One may then formally reexpress Eq. (3) in terms of these signal-averaged values as

$$\sigma_{n\xi}^2 = \sigma_{nx}^2 + \sigma_{ny}^2 - 2\rho_{nc}\sigma_{nx}\sigma_{ny}, \tag{5}$$

where σ_{nx} and σ_{ny} represent the normalized standard deviation of the Γ/n signal-averaged data points from lasers x and y, respectively, and ρ_{nc} is the cross correlation of pairs of these same signal averaged data.

It is particularly important to note that since σ_{nx} and σ_{ny} have been determined from data averaged over n pulses, $\sigma_{n\xi}$ corresponds to the normalized standard deviation of the ratio of the returns from the two lasers after averaging these lidar signals from each laser over the corresponding n pulses. That is, one averages first and then takes the ratio. This averaging then acts as a low-pass filter, reducing the effect of high-frequency fluctuations, i.e., those occurring on a time scale that is short compared with the time required to produce the n pulses being averaged. It should be noted that using the opposite order of taking the ratio of the individual pulse pairs first and then averaging, while permissible in general, would be incorrect in the context of Eq. (5) since the terms on the right-hand side of that equation refer to averaged values. In addition, taking ratios first may seriously bias the result[28] (where bias refers to the difference between the mean value of the estimator and the measured value) because of the accentuated effect of small fluctuations of the individual signals on their ratio. This point is addressed more fully in Sec. IV.B.2.

The terms on the right-hand side of Eq. (5) may be related directly to the individual lidar returns. Specifically, the relationship between the standard deviation of the mean of the returns from lasers 1 and 2, σ_{nx} and σ_{ny}, and their respective temporal autocorrelation functions is given by Eq. (4). The relationship of the effective pulse-averaged temporal cross-correlation coefficient ρ_{nc}, with the pulse-pair value ρ_c and with the temporal cross-correlation coefficients of the lasers ρ_{xy}, for delay times of the order of $j\tau$ is derived in Appendix A and shown to be

$$\rho_{nc} = \frac{\sigma_x\sigma_y}{n\sigma_{nx}\sigma_{ny}}\left[\rho_c + 2\sum_{j=1}^{n-1}(1 - j/n)\rho_{xy}\right], \tag{6}$$

where the explicit definition of ρ_{jxy} is shown in Eq. (A5) to be

$$\rho_{jxy} = \frac{1}{\sigma_x\sigma_y(\Gamma - j)}\sum_{k=1}^{\Gamma-j} I_{kx}I_{(k+j)y} \tag{7}$$

Using the values of σ_{nx} and σ_{ny} given by Eq. (4), one may rewrite Eq. (6) as

$$\rho_{nc} = \frac{\left[\rho_c + 2\sum_{j=1}^{n-1}(1 - j/n)\rho_{xy}\right]}{\left[1 + 2\sum_{j=1}^{n-1}(1 - j/n)\rho_{xx}\right]^{1/2}\cdot\left[1 + 2\sum_{j=1}^{n-1}(1 - j/n)\rho_{yy}\right]^{1/2}}. \tag{8}$$

Equations (6) and (8) relate the signal-averaged cross-correlation coefficient ρ_{nc} to the autocorrelation functions of the individual lidar returns, ρ_{jx} and ρ_{jy}, and to the cross-correlation values ρ_c and ρ_{jxy}.

Although Eq. (8) defines the functional relationship between ρ_{nc} and the fundamental parameters (ρ_{jx}, ρ_{jy}, ρ_c, and ρ_{jxy}), it should be noted that the behavior of these fundamental parameters is strongly dependent on experimental conditions and difficult to predict accurately from first principles. Measurements which validate Eqs. (6) and (8) and describe the behavior of these fundamental parameters in different experimental conditions are presented in the following section.

IV. Experiments

In this section, we present the results of experiments which directly measured the improvement in measurement accuracy that can be obtained under various experimental conditions by using a dual-laser DIAL system in conjunction with signal averaging. By experimentally measuring $\sigma_{n\xi}$ and ρ_{nc} and comparing the results obtained with those predicted by the theoretical analysis of the previous section, we established the validity of Eq. (8) and determined the limits of validity of Eqs. (3) and (5). The analysis also provides a theoretical framework for understanding some of the observed limitations in the ability of signal processing to reduce DIAL measurement uncertainties in these experiments.

A. Experimental Apparatus and Technique

A schematic of the dual CO_2 laser DIAL system used in these experiments is shown in Fig. 1. A detailed description of the system has been presented previously.[15] The system employs two line-tunable hybrid mini-TEA CO_2 lasers[29] which provide single-frequency pulsed radiation. The two lasers are separately triggered, with a time delay Δt between firing of the two lasers. The value of Δt was maintained at 5–7 μsec in the experiments described below; over this short time interval the atmosphere is effectively frozen. The beam paths of the two lasers are joined at a 50/50 beam splitter. The transmitted beam was expanded to a 6-cm diameter, and the receiver is a 25-cm Cassegrain telescope. The detection system includes two independent HgCdTe detector units, which permit both

employed, much shorter decorrelation times have been measured. Experiments carried out with $\Delta t \ll 1$ msec have shown that the value of ρ_c between pulse-pair signal returns depends strongly on both the nature of the reflective target and the detection mode.[22,25,26] In general, good agreement between the measured value of σ_ξ and that predicted by Eq. (3) is usually obtained. However, it should be noted that the derivation of Eq. (3) involves a Taylor series expansion and is correct only to first order. The validity of the equation is, therefore, limited to cases where higher-order terms are negligible.

B. Signal Averaging

Signal averaging may be used to reduce the value of the standard deviation of the lidar returns from each laser in Eq. (3). For n measurements, the normalized standard deviation of the mean σ_n should decrease as $n^{-1/2}$ assuming the measurements are independent. However, experimental DIAL measurements have shown strong departures from $n^{-1/2}$ behavior,[18] indicating that successive lidar returns were not independent but were temporally correlated. These experimental results were shown to agree with a theoretical[19] study which established the relationship between σ_n and temporal autocorrelation as

$$\sigma_n = \frac{\sigma}{\sqrt{n}}\left[1 + 2\sum_{j=1}^{n-1}(1 - j/n)\rho_j\right]^{1/2}. \tag{4}$$

In Eq. (4), σ is the normalized standard deviation of the full set of individual signals, and ρ_j is the temporal autocorrelation function for a delay time $j\tau$, where τ is the time interval between pulses of each individual laser; the autocorrelation function is defined in Appendix A. On the basis of Eq. (4), it can be shown that small temporal autocorrelation effects among successive laser pulses severely limits the improvement available by signal averaging.[19] In the absence of temporal autocorrelation, Eq. (4) reduces to the usual $n^{-1/2}$ behavior.

To avoid confusion, one should note the difference between the cross-correlation coefficient ρ_c in Eq. (3) and the autocorrelation function ρ_j in Eq. (4). Cross correlation refers to the temporal correlation of the pulse-paired returns from lasers 1 and 2, while autocorrelation refers to the correlation of successive pulse returns from each individual laser.

C. Physical Processes Relating Lidar and Signal Processing Parameters

Before continuing with the signal processing analysis, it is worthwhile to consider the physical mechanisms which relate the fluctuations of the return lidar signals P_1, P_2, and P', as given in Eqs. (1) and (2), with the signal processing parameters of Eqs. (3) and (4). Our discussion will be qualitative rather than quantitative. Quantitative predictions can be made under assumed ideal conditions[7] but are beyond the scope of this paper.

As seen from Eq. (1), the statistical and temporal behavior of the return signals are dependent on the target reflectivity characteristics ρ and the atmospheric attenuation effects α, each of which has associated statistical fluctuations and temporal correlation properties. The fluctuations arise as the result of speckle effects at the target, atmospheric effects in the form of turbulence or relatively long-term atmospheric absorption drifts, and experimentally induced fluctuations due to laser beam pointing jitter, laser frequency jumps, or noise processes associated with the optical detection system.

It is the interplay of all these physical effects on ρ and α which determines the statistical and temporal characteristics of P and P' and hence the values of σ_x, σ_y, ρ_c, and ρ_j. Since the individual effects giving rise to fluctuations will have different spatial and temporal characteristics, one may reasonably predict that the relative effectiveness of different signal processing techniques will depend strongly on the nature of the conditions under which a DIAL measurement is carried out. For example, heterodyne detection of atmospheric lidar backscatter from aerosols results in short-term speckle-induced fluctuations of the reflectivity term ρ with decorrelation times of the order of 1 μsec.[24] Under these conditions the cross-correlation coefficient ρ_c would be expected to be near zero and should, therefore, be a minor factor in reducing measurement uncertainty. However, during the time period required for signal averaging over a large number of pulses, the return signals will be influenced by the turbulence-induced fluctuations in α with decorrelation times of the order of 1 msec,[22,23] or the even longer-term changes in α due to atmospheric drift. In this case, $\rho_c > 0$ and can lead to a significant reduction in the overall uncertainty of a ratio measurement relative to the uncertainties of the individual measurements. In addition, both short- and long-term temporal effects will also influence the autocorrelation coefficient ρ_j.

Although the theories of speckle and propagation through turbulence are well understood,[27] it remains difficult to take all the factors occurring simultaneously into account with sufficient accuracy to make an accurate prediction of these values *a priori* for a given lidar system. However, these theories provide a basis for a qualitative discussion of the results to be expected under various experimental conditions. The lidar experiments described in this paper provide information regarding the relative effectiveness of signal processing techniques for improving the accuracy of DIAL measurements under different experimental conditions. It is also hoped that the results will provide insights leading to a more complete understanding of the physics involved in laser remote sensing.

III. Analysis

The relationship between the signal return ratios and the temporal cross-correlation coefficient, as given in Eq. (3) for pulse pairs, may be extended to incorporate signal averaging. Combining both temporal cross correlation and signal averaging involves expressing the dual-laser DIAL relationship, Eq. (3), in terms of the signal averaged values of the individual lasers and their

the theoretical analysis. These results are used to study the relative merits of single- and dual-laser lidar systems and to help establish the limits of accuracy improvement achievable with DIAL measurements by the use of different signal processing techniques.

It should be noted that this theoretical analysis relates quantities which are experimentally measured and is used to provide insight into the relative magnitude of the effects of different lidar processes on the overall accuracy of a DIAL measurement. The analysis does not predict the value of the basic quantities, such as lidar fluctuation levels and atmospheric correlation times; such values are difficult to predict from first principles except under selected idealized conditions.

A brief review of our previous analysis of the effects of signal averaging and temporal cross correlation considered separately is given in Sec. II. A theoretical analysis which combines the effects of signal averaging and temporal cross correlation within a single analytical framework is presented in Sec. III. This is followed in Sec. IV by a description of experiments carried out with the dual-CO_2 laser DIAL system to obtain the signal-averaged variance of the lidar returns from the individual lasers and of their ratio. The experimental results are shown to be in good agreement with those predicted on the basis of the theoretical analysis given in Sec. III. Results are also used to help determine the limits of validity of the theoretical analysis and to establish the relative merits of different experimental techniques for the various experimental conditions considered. Conclusions based on the results of these experiments and the analysis are given in Sec. V.

II. Review

The lidar equation for the path-averaged laser remote sensing of a molecular constituent in the atmosphere using backscatter from a hard target located a distance R from the lidar system is given by

$$P_r = (P_t K \rho A / \pi R^2) \exp[-2(\sigma_a N_a + \alpha)R], \quad (1)$$

where P_r is the instantaneous received optical power of the backscattered lidar radiation after reflection from the target, P_t is the transmitted power, K is the system optical efficiency, ρ is the target reflectivity, A is area of the receiving telescope, σ_a is the absorption cross section of the molecule being investigated, N_a is the average concentration of the absorbing molecule over the range R, and α is the atmospheric extinction coefficient.

In a DIAL measurement, backscattered lidar returns are obtained at two frequencies, ν and ν', which correspond to high- and low-absorption frequencies of the molecular species investigated. In that case, the concentration of the species is deduced from the ratio of the lidar returns at the low- and high-absorption frequencies of the species investigated rather than from the individual returns according to the relationship

$$N_a = \ln(P'/P)/2(\sigma_a' - \sigma_a)R, \quad (2)$$

where $P = P_r/P_t$ is the received signal power normalized to the transmitted power, and the primed and unprimed parameters correspond to values obtained at the low- and high-absorption frequencies, respectively.[21]

It is clear that fluctuations in the lidar signal returns, P and P', will affect the accuracy with which the species concentration N_a may be determined experimentally. It was noted in Sec. I and the experimental data will show that the fluctuation levels of P and P' are greatly influenced by the detection mode employed. This is due to the fact that in direct detection the return lidar signal is proportional to the square of the electric field amplitude integrated over the detector field of view; that is, $P(\text{direct}) \propto \int E^* E\, dA$; in this case changes in the complex phase factor are eliminated. However, for heterodyne detection, P is proportional to the integral of the product of the electric field amplitude of the return signal beam and the local oscillator field, $P(\text{heterodyne}) \propto \int E_{LO} E^* dA$. Therefore, phase factors have a pronounced effect on the signal fluctuation levels of heterodyne-detected lidar returns.

Studies have been made of the extent to which measurement uncertainties due to the fluctuation of lidar returns may be reduced either by using a dual-laser system to take advantage of cross-correlation effects or by signal averaging. Results of the studies are briefly reviewed in turn in the following section.

A. Temporal Pulse-Pair Cross Correlation in a Dual-Laser System

It is sometimes possible to reduce the DIAL measurement uncertainty by taking advantage of atmospherically induced temporal cross correlation to reduce the fluctuations of the ratio of these returns. However, to achieve this, the laser beam pulses at ν and ν' must be separated by a time period which is short compared with the decorrelation time of atmospheric turbulence ($\sim$1 msec).[22] This can be accomplished by using two lasers in a dual-laser system to provide two nearly simultaneous beams operating along the same path. With lasers 1 and 2 operating at frequencies ν and ν', respectively, it has been found that the normalized variance of the ratio of the return signals is approximately related to that of the individual return values by[20]

$$\sigma_\xi^2 = \sigma_x^2 + \sigma_y^2 - 2\rho_c \sigma_x \sigma_y, \quad (3)$$

where σ_x and σ_y are the standard deviations of the lidar return signals of lasers 1 and 2, respectively, normalized by their respective mean values, σ_ξ is the normalized standard deviation of the ratio of the returns ($\xi = x/y$), and ρ_c is the temporal pulse-pair cross correlation of the returns from the two lasers; σ_ξ, σ_x, and σ_y are measures of the uncertainty in the determination of P/P', P, and P', respectively. It is seen in Eq. (3) that a positive value of ρ_c results in a reduced DIAL measurement uncertainty σ_ξ.

Experimentally, large values of ρ_c have been obtained for pulse-paired lidar signals reflected from stationary targets when the time separation Δt between the pulse pairs is of the order of or $<$1 msec. Atmospheric effects due to turbulence may be considered frozen over this interval.[22,23] When a moving target[24] or source[25] is

Reprinted from Applied Optics, Vol. 24, page 118, January 1, 1985

Error reduction in laser remote sensing: combined effects of cross correlation and signal averaging

Norman Menyuk, Dennis K. Killinger, and Curtis R. Menyuk

A systematic analysis is presented of the extent to which the accuracy of a differential-absorption lidar (DIAL) measurement may be improved by using the combined effects of signal averaging and temporal cross correlation. Previous studies which considered these effects separately are extended by incorporating both effects into a single analytical framework. In addition, experimental results involving lidar returns from a diffusely reflecting target using a dual-CO_2 laser DIAL system with both heterodyne and direct detection are presented. These results are shown to be in good agreement with the theoretical analysis and help establish the limits of accuracy achievable under various experimental conditions.

I. Introduction

Differential-absorption lidar (DIAL) systems have been used extensively for the single-ended remote sensing measurement of molecular species in the atmosphere.[1] Such measurements involve use of atmospheric extinction and backscatter of laser radiation at two distinct frequencies, where the frequencies are normally chosen to coincide with high and low absorption of the molecule being investigated. The concentration of the molecular species is deduced from the difference in the measured values of the backscattered laser signal returns at the two frequencies.

These returns are subject to several noise sources, including those added by the detection process, such as shot noise in the case of heterodyne detection or dark current and background noise for direct detection. These noise sources generally define the ultimate measurement capability of a DIAL system.[2-4] However, lidar signals traveling through the atmosphere are also subject to significant pulse-to-pulse temporal fluctuations due to several factors operating on the laser beam during its round trip from transmitter to receiver. These factors include extinction and scintillation effects of atmospheric turbulence,[5-7] speckle or glint effects at the reflective target,[7,8] and laser beam wander due to either atmospheric turbulence or the laser source.[10,11] In addition, since the heterodyne- and direct-detection modes are dependent on the amplitude and phase of the lidar signal in different ways, the detection mode will also influence the resultant SNR and fluctuation level observed.[2-4,12-15] In many cases, notably when the average signal return is significantly greater than the average detector noise level, it is the pulse-to-pulse fluctuation which limits the measurement accuracy of the average lidar return signal and is, therefore, the factor that limits the accuracy with which the molecular species concentration can be determined with a DIAL system.[16,17]

Previous analyses and experimental studies investigated the extent to which the accuracy of a DIAL measurement may be improved through use of two separate techniques, namely, by signal averaging of the lidar returns[18,19] or by using a dual-laser DIAL system to exploit the fact that on a sufficiently short time scale, both laser beams may effectively see the same atmospheric fluctuations.[20] In this paper, we extend these studies by incorporating both techniques within a single analytical framework which effectively combines the influence of both signal averaging and temporal cross correlation. This extension involves a theoretical analysis which relates the signal-averaged statistical DIAL measurement error and the temporal autocorrelation and cross correlation of the individual lidar pulses. The theoretical predictions based on this analysis were compared with extensive experimental measurements obtained using both heterodyne- and direct-detection CO_2 lidar systems. The DIAL experiments measured the statistical error, autocorrelation, and cross correlation of the DIAL returns. These experimental results were then compared with those predicted by the theoretical analysis. In general, the experimental results are shown to agree with results of

C. R. Menyuk is with University of Maryland, Laboratory for Plasma & Fusion Energy Studies, College Park, Maryland 20742; the other authors are with MIT Lincoln Laboratory, Lexington, Massachusetts 02173-0073.

Received 6 July 1984.
0003-6935/85/010118-14$02.00/0.

Appendix A

The following is a reprint of a journal article published in Applied Optics, 1 January 1985, entitled "Error Reduction in Laser Remote Sensing: Combined Effects of Cross Correlation and Signal Averaging".

REFERENCES

1) D. K. Killinger, N. Menyuk and A. Mooradian, private communication.

2) W. S. Benedict and R. F. Calfee, "Line Parameters for the 1.9 and 6.3 Micron Water Vapor Bands," ESSA Professional Paper 2, U.S. Dept. of Commerce (1967).

3) P. Moulton, private communication.

nitrogen which produced large optical distortion, and it was felt that a more careful design of the cavity would alleviate these problems.

VII. SUMMARY AND CONCLUSION

The results presented in this report have described progress which has been made in the development and measurement of the 1.7μm Co:MgF_2 DIAL system, and results obtained using the CO_2 DIAL system for the remote sensing of atmospheric ammonia.

The CO_2 DIAL measurements indicated that NH_3 may be present in the atmosphere at concentrations as high as 30 ppb, and appears to exhibit an inverse dependence on the water vapor aerosol concentration. The investigation of the effects of signal averaging and temporal processes in the atmosphere indicated an accuracy on the order of a few percent for direct-detection and on the order of 10 to 20 percent for heterodyne detection.

The Co:MgF_2 DIAL system has been shown to offer significant potential for the remote sensing of HCl in the atmosphere. Further investigations are planned using calibration sources of HCl in order to establish the sensitivity of the Co:MgF_2 DIAL system for both path-averaged and range-resolved results.

returns, one deduces that the path-averaged sensitivity of the DIAL system was approximately 0.2 ppm of HCl over the 3 km range.

VI. INITIAL INVESTIGATIONS OF FREQUENCY SHIFTING Co:MgF_2 LASER

Three frequency-shifting techniques were theoretically studied by P. Moulton.[3] They were (1) difference-frequency generation using a Nd:YAG and Co:MgF_2 laser, (2) Co:MgF_2 laser pumped optical parametric oscillator using a $AgGaSe_2$ crystal, and (3) Raman shifting the Co:MgF_2 laser to longer wavelengths. The first two techniques were not experimentally investigated because (1) the temporal overlap of the Nd:YAG laser pulse and Co:MgF_2 laser pulse is very small since pulsewidths for a relatively energetic Q-switched Nd:YAG laser are typically 10 ns, which is much shorter than the Q-switched Co:MgF_2 laser pulse of 500 ns, and (2) large (> 0.5 cm) $AgGaSe_2$ crystals are not commercially available at this time. Because of these limitations, only the Raman-shifting technique was experimentally investigated.

Initial Raman-shifting was attempted using the Co:MgF_2 laser focused into a $\lambda/4$ waveplate-isolated, single-pass, Raman cell containing liquid nitrogen. Results of this experiment were negative, because of the low power of the Co:MgF_2 and the high-threshold of single-pass stimulated Raman scattering (SRS).

An additional experiment was attempted to observe low threshold SRS using liquid nitrogen in an optical cavity. Calculations indicated that SRS should have been above threshold; however, no signal was observed. This negative result is believed to have been caused by thermal gradients in the liquid

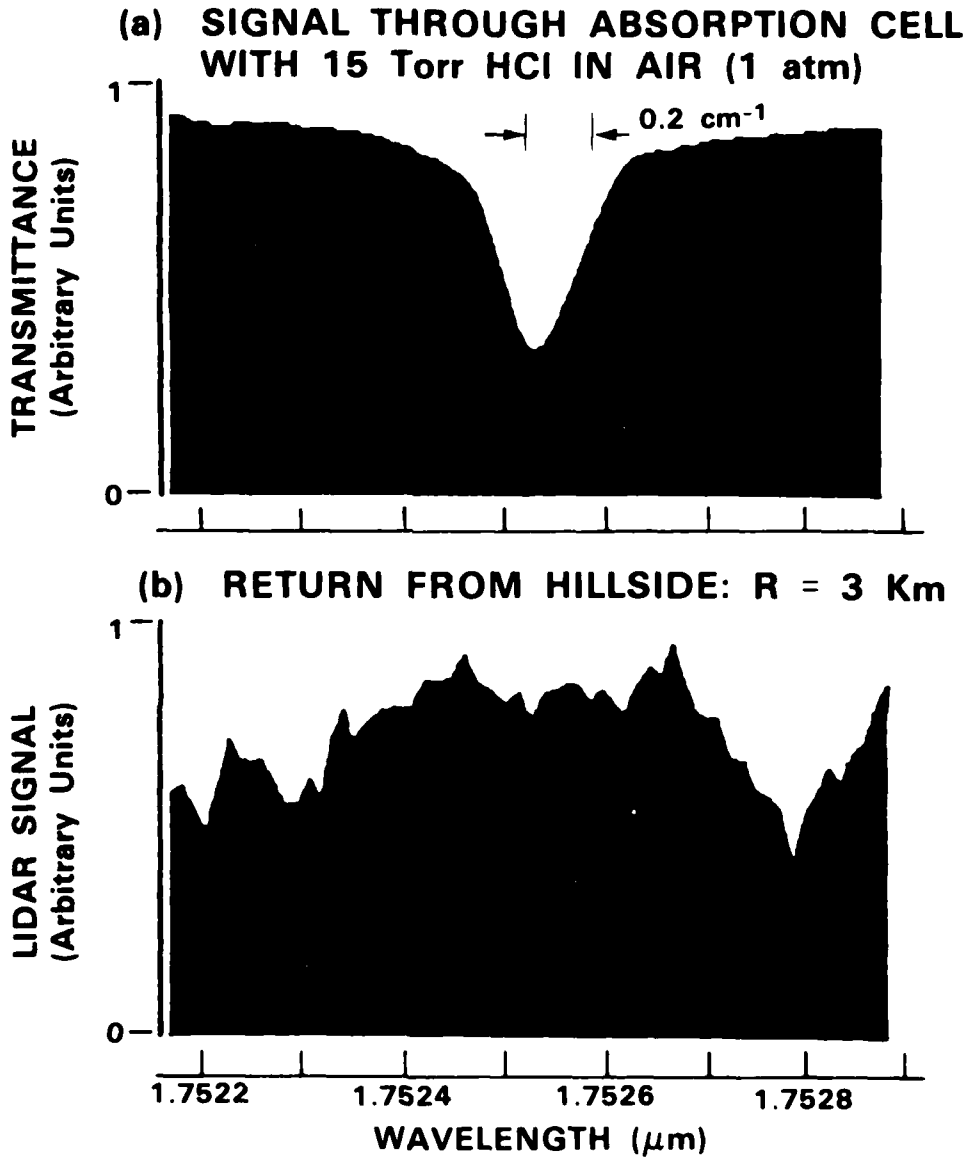

Figure 6. Wavelength scan of Co:MgF_2 LIDAR over HCl absorption line.

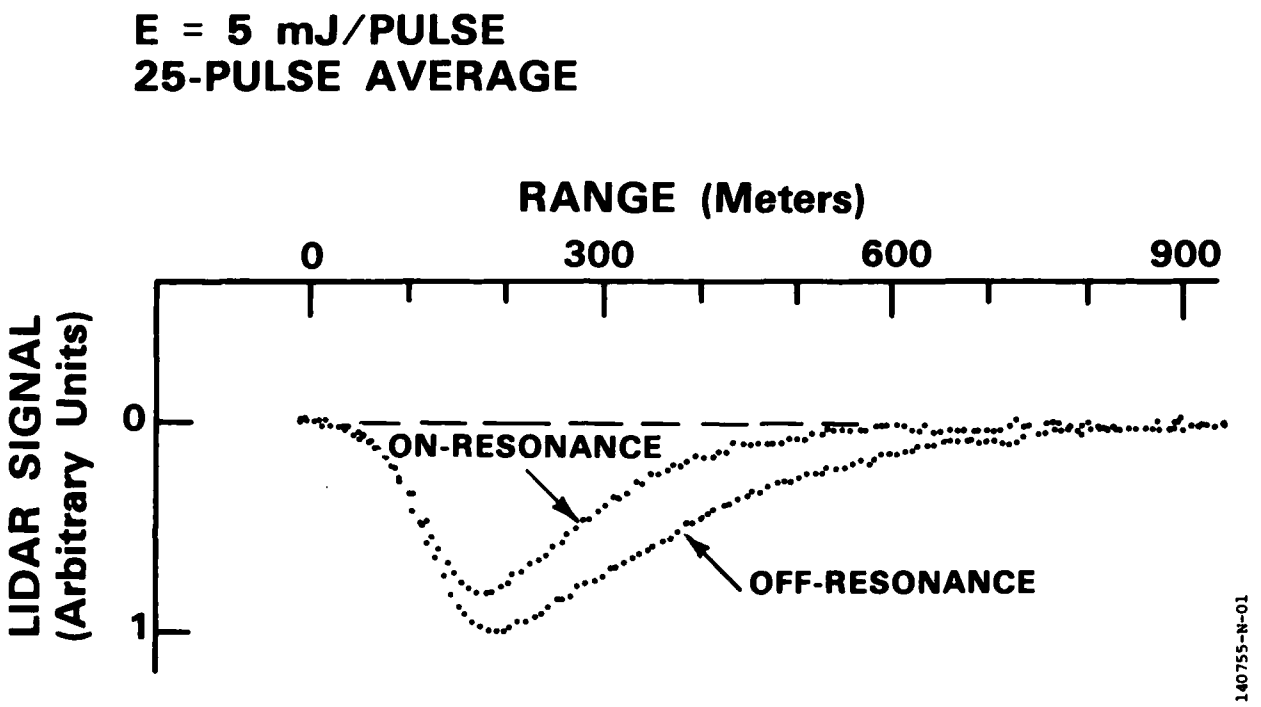

Figure 5. Co:MgF_2 LIDAR aerosol backscatter.

Figure 5 shows the range-resolved LIDAR returns as the laser was tuned on- and off-resonance through a strong water vapor line near 1.7515 μm. With an expected absorption coefficient of 8.3×10^{-3} $(\text{atm cm})^{-1}$, one deduces from the observed differential signal near 300 m in Fig. 5 that approximately 2.5 Torr of water vapor was present. This number is in approximate agreement with that actually measured using the wet-bulb/dry-bulb thermometer.

Considerable scatter was observed in the range-resolved returns at ranges greater than 500 meters due to the low signal-to-noise ratio for the absorbed on-resonance signal. Further work is being conducted to improve this detection range by increasing the power of the laser system.

V. REMOTE SENSING OF HCl

The Co:MgF_2 DIAL system was used for the path-averaged remote sensing of HCl in the atmosphere. Laboratory absorption data and atmospheric DIAL data were collected as the Co:MgF_2 laser was tuned through an HCl absorption line near 1.7525 μm; this absorption is a first overtone ($v = 0 \rightarrow 2$) transition.

Figure 6 shows the absorption spectrum obtained for both the 105-cm-long absorption cell containing 15 Torr of HCl in air and, simultaneously, the LIDAR returns obtained from a hillside at a range of 3 km. One deduces from the observed 60% peak absorption due to HCl in Fig. 6a that the absorption coefficient, σ, for this line is 0.45 $(\text{atm cm})^{-1}$, in good agreement with previous results.[1]

As evident in Figure 3, no obvious HCl absorption feature is observed in the DIAL spectrum. With a 5% uncertainty in the noise background of the DIAL

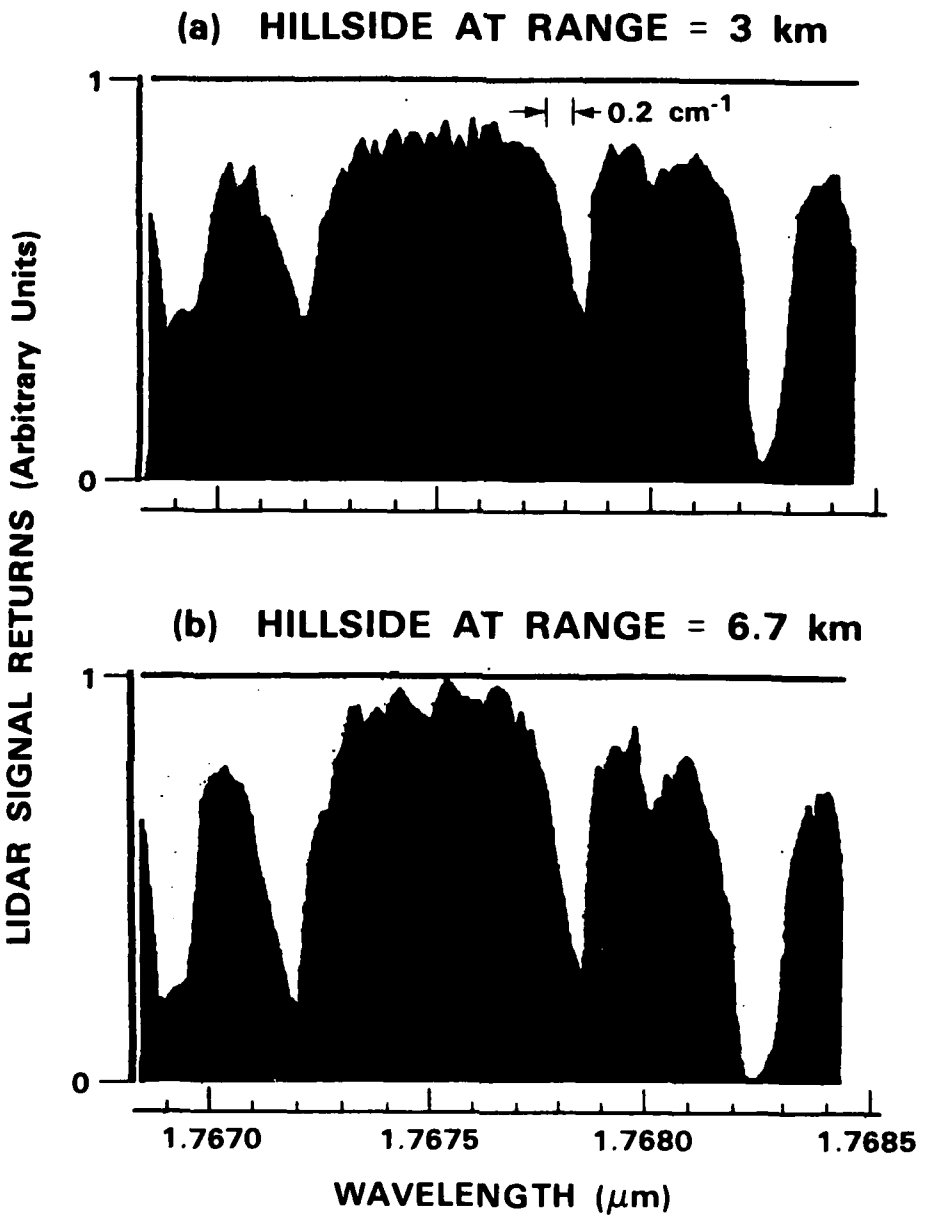

Figure 4. Wavelength scan of Co:MgF_2 LIDAR returns.

laser pulses. Each LIDAR return was normalized to the transmitted laser energy per pulse. The range-resolved concentration of the species was then computed and displayed on the graphics computer terminal.

IV. INITIAL RANGE-RESOLVED Co:MgF_2 MEASUREMENTS

The Co:MgF_2 DIAL system was used to measure the path-averaged and range-resolved concentration of water vapor in the atmosphere. These measurements were used to establish the capability and sensitivity of the DIAL system.

Path-averaged DIAL measurements were made using the backscattered DIAL returns from a hillside at a range of 3 km and 6.7 km. Figure 4 shows the DIAL returns as the laser wavelength was tuned through several water vapor lines near 1.767 μm. The isolated water vapor line near 1.7679 μm has an expected peak absorption coefficient, σ, of 5.2×10^{-4} $(atm\text{-}cm)^{-1}$ and a linewidth of 0.1 cm^{-1}.[2] With the observed 52% absorption of this line in Fig. 4, one calculates a water vapor pressure of 0.0023 atmospheres (1.8 Torr).This value is a factor of two less than that actually present as measured by a wet-bulb/dry-bulb thermometer which indicated 0.0048 atmospheres of water vapor. This discrepancy in the determined DIAL H_2O concentration is attributable to the finite linewidth of the Co:MgF_2 laser (0.15 cm^{-1}) which serves to reduce the peak absorption strength and to broaden the measured absorption line, as seen in Fig. 4. Further study of this reduction is planned.

Preliminary range-resolved atmospheric DIAL measurements were made with the weak backscattered returns from naturally occurring aerosols in the atmosphere. LIDAR returns were detected at ranges out to 700 meters.

most continuous increase in the magnitude of the return signals from both lasers indicative of a decreasing atmospheric extinction. The results obtained under both sets of atmospheric conditions are described in the succeeding sections. These experiments were performed with laser 1 operating on the 10.6-μm $P(22)$ laser transition and laser 2 operating on the 10.7-μm $P(28)$ transition.

In general, it is desirable to have the frequencies of the two lasers as close together as possible to minimize the decorrelation due to turbulence-induced scintillation[6,7] and speckle effects at the target. For the frequency difference between the $P(22)$ and $P(28)$ transition and, in general, for other frequency differences within the range of CO_2 lasers, decorrelation effects due to $\Delta\nu$ in direct detection was found to be small but not negligible. Specifically, it was shown that $\rho_c \approx 0.45$ for $\nu = \nu'$,[22] while for $\nu \neq \nu'$ we have observed $\rho_c \approx 0.3$–0.4. This contrasts strongly with decorrelation effects which occur when heterodyne detection is used. In that case, speckle effects at the target cannot be averaged, which results in a strong decorrelation when $\nu \neq \nu'$. This is discussed more fully in Sec. IV.B.2.

1. Varying atmospheric extinction. The values measured for the standard deviation of the mean of lasers 1 and 2, σ_{nx} and σ_{ny}, and of their ratio $\sigma_{n\xi}$ for n = 1,2,4,8, . . . , 512 are shown in Fig. 2(a) for the case where the atmospheric extinction was slowly decreasing over the 10-min period during which the measurement was carried out. The values of $(\sigma_{nx}^2 + \sigma_{ny}^2)^{1/2}$ are also given since they represent the effective standard deviation of the measurement in the absence of cross correlation. In effect, these values represent the expected standard deviation, or measurement uncertainty, of a DIAL system which uses a single laser switching between the on- and off-resonance frequencies.

There are several features of interest in the results shown. They are as follows: (1) the reduction of σ_{nx}, σ_{ny}, and $\sigma_{n\xi}$ with n is significantly slower than $n^{-1/2}$; (2) for n = 1, there is a slight improvement in measurement accuracy using a dual-laser system to obtain the ratio value σ_ξ relative to $(\sigma_x + \sigma_y^2)^{1/2}$, consistent with a small positive value of ρ_c and Eq. (3); and (3) the improvement in the ratio value $\sigma_{n\xi}$ relative to $(\sigma_{nx}^2 + \sigma_{ny}^2)^{1/2}$ is seen to increase continuously with increasing n, indicating that ρ_{nc} is increasing with increasing n.

In general, the measured values of $\sigma_{n\xi}$ shown in Fig. 2(a) were in excellent agreement with the theoretical values calculated using Eq. (5). In addition, the functional relationships involving the autocorrelation and cross-correlation coefficients were found to agree with the theoretical analysis as presented in Eqs. (6) and (8).

Since the behavior of the fundamental parameters (ρ_{jx}, ρ_{jy}, ρ_c, and ρ_{jxy}) are strongly dependent on experimental conditions, a detailed discussion of the physical mechanisms giving rise to the observed functional forms of these parameters is considered below.

The slow reduction of σ_{nx} and σ_{ny} with increasing n is due to the presence of temporal autocorrelation, ρ_{jx} and ρ_{jy}, in the lidar returns from lasers 1 and 2, respectively, as shown in Fig. 2(b) for j = 1,2,4,8, . . . , 512, where the temporal cross correlation ρ_{jxy} is also given. The autocorrelation function is unusually large in this case, apparently due to the presence of the slow atmospheric drift during the measurement period. This results in the observed long-term temporal correlation that remains essentially unchanged over time delays from 1.6 to 50 sec. The measured relationship between the standard deviation of the mean for the two sets of laser returns and the autocorrelation functions is in agreement with Eq. (A6).

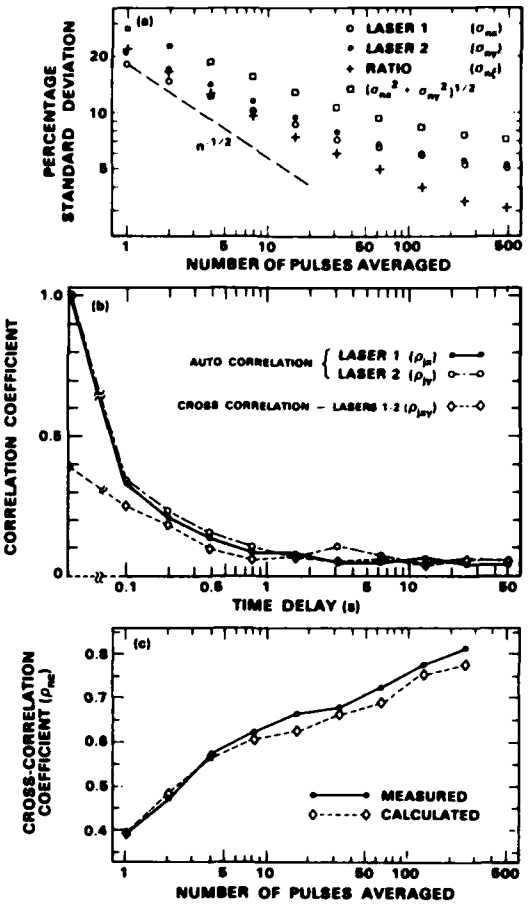

Fig. 2. Lidar signal return data from diffusely reflecting target at a 2.7-km range using direct detection during period of continuously decreasing atmospheric extinction: (a) standard deviation of returns from lasers 1 and 2 and their ratio as functions of the number of pulses averaged; (b) temporal autocorrelation and cross correlation of laser return signals as functions of time delay; and (c) comparison of measured and calculated values of signal-averaged cross-correlation coefficient as a function of the number of pulses averaged.

As noted above, the increasing ratio of $\sigma_{n\xi}$ relative to $(\sigma_{nx}^2 + \sigma_{ny}^2)^{1/2}$ with increasing n is consistent with a value of ρ_{nc} that increases continuously with increasing n. The measured values of ρ_{nc} vs n is given in Fig. 2(c), and just such an increase is observed. In addition, the values of ρ_{nc} were calculated on the basis of Eq. (8) using the values of ρ_{jx}, ρ_{jy}, and ρ_{jxy} shown in Fig. 2(b) and assuming a linear intepolation for all other values of j. The calculated values of ρ_{nc} are also given in Fig. 2(c)

and are seen to be in good agreement with the measured values. The reason for the observed increase of ρ_{nc} with n is discussed below.

The observed variation of ρ_{nc} with n cannot be ascribed to the effective low-pass frequency-filtering effect of averaging over the n pulses, since that effect is similar in both the numerator and denominator in Eq. (8). To illustrate this point, let us make the simplifying *a priori* assumption $\rho_{jx} = \rho_{jy}$. Then Eq. (7) becomes

$$\rho_{nc} = \frac{\left[\rho_c + 2\sum_{j=1}^{n-1}(1 - j/n)\rho_{jxy}\right]}{\left[1 + 2\sum_{j=1}^{n-1}(1 - j/n)\rho_{jx}\right]}. \tag{9}$$

The experimental results of Kjelaas *et al.*[6] indicate that the temporal cross-correlation coefficient ρ_{jxy} is proportional to the temporal autocorrelation coefficient ρ_{jx}; i.e., $\rho_{jxy} = K\rho_{jx}$. However, if this proportionality constant is extrapolated back to a zero time delay, one would obtain $K = \rho_c$, and Eq. (9) would then become $\rho_{nc} = \rho_c$, which clearly disagrees with experimental results.

This apparent discrepancy, which arises when the proportionality constant is extrapolated back to zero, is due to the role noise plays in the averaging process for autocorrelation and cross correlation. In general, lidar return signals contain both a true signal and a noise component. The noise components of the two lasers are uncorrelated with each other. Therefore, in the averaging process given in Eqs. (A4) and (A5) the effect of the noise will effectively be reduced or eliminated. The effect of noise will be similarly reduced or eliminated in temporal autocorrelation measurements by the averaging process given by Eq. (A3) when the time delay $j\tau$ is greater than the coherence time of the noise component. The results of Kjelaas *et al.*[6] indicate that this coherence time is <2 msec; for delays greater than this, the expression $\rho_{jxy} = K\rho_{jx}$ can be expected to hold to within experimental uncertainties. However, for zero time delay, i.e., $j\tau = 0$, $\langle I_x(t_k)I_x(t_k + j\tau)\rangle$ in Eq. (A3) becomes $\langle I_x(t_k)^2\rangle$. Since $I_x(t_k)$, which corresponds to the kth lidar signal return, includes a noise component $\langle I_x(t_k)^2\rangle$ will yield a noise-squared term which is not eliminated during the averaging process. Hence the zero time delay autocorrelation coefficient, which is by definition equal to unity, uniquely contains a significant noise component after signal averaging. Therefore, $\rho_c < \rho_{jxy}/\rho_{jx}$, or $K = \zeta\rho_c$, where $\zeta > 1$. With this further modification, Eq. (9) becomes

$$\rho_{nc} = \frac{\rho_c\left[1 + 2\zeta\sum_{j=1}^{n-1}(1 - j/n)\rho_{jxy}\right]}{\left[1 + 2\sum_{j=1}^{n-1}(1 - j/n)\rho_{jx}\right]}. \tag{10}$$

Equation (10) gives insight into the physical mechanism which may yield a rising value of ρ_{nc} with increasing n as long as $\rho_{jxy} > 0$. The equation indicates it is the fact of $\zeta(>1)$ multiplied by the summation term in the numerator which causes this increase. Therefore, a summation term which remains positive out to longer time-delay periods will result in a greater increase in ρ_{nc}. This is just the situation which occurs in the case of long-term atmospheric drift.

A necessary condition for this explanation to be valid is that there be a significant increase in the ratio of the cross correlation to autocorrelation on going from a zero time delay to $j = 1$. It is seen in Fig. 2(b) that there is an ~65–70% decrease in the autocorrelation on going from zero delay to the delay time associated with $j = 1$ (0.1 sec), while the corresponding decrease for the cross correlation is only 30%. This is in accord with the model proposed (i.e., $\zeta > 1$) to explain the observed variation of ρ_{nc} with n.

It should be noted that Eqs. (9) and (10) involved simplifying assumptions which are not strictly true. In general, as we have seen, $\rho_{jx} \neq \rho_{jy}$, and there is considerable scatter in the experimental values of ρ_{jx}, ρ_{jy}, and ρ_{jxy}. Therefore, any direct comparison with experiment must be made using Eq. (8).

2. Constant average atmospheric extinction. A second similar experiment carried out over a period during which the average atmospheric extinction remained essentially constant led to the results in Figs. 3(a), (b), and (c). They show both important similarities with and marked differences from the corresponding results described above and shown in Figs. 2(a), (b), and (c), respectively.

Comparison of the results shown in Fig. 3(a) with those of Fig. 2(a) indicate the following significant differences in behavior: (1) although the reduction of σ_{nx} and σ_{ny} with n remains considerably slower than $n^{-1/2}$, the variation is significantly more rapid than was observed for the varying extinction case, and, (2) the improvement in measurement accuracy obtainable using $\sigma_{n\xi}$ relative to $(\sigma_{nx}^2 + \sigma_{ny}^2)^{1/2}$ is seen to increase with increasing n to $n = 8$ and then to decrease, in marked contrast with the constantly increasing improvement with increasing n observed in Fig. 2(a).

The more rapid decrease of σ_{ns} and σ_{ny} with n for the constant average extinction is consistent with the more rapid decrease of the autocorrelation functions with increasing time delay j for this case, as seen in Fig. 3(b). The relationship between the standard deviation of the mean for each of the lasers, σ_{nx} and σ_{ny}, and ρ_{jx} and ρ_{jy}, respectively, are in agreement with Eq. (A6).

The measured values of the signal-averaged cross-correlation coefficient ρ_{nc} as defined by Eq. (A7) is shown as a function of n in Fig. 3(c). In addition, the values of ρ_{nc} were calculated on the basis of Eq. (7) using the values of ρ_{jx}, ρ_{jy}, and ρ_{jxy} given in Fig. 3(b) and assuming a linear interpolation for all other values of j. These calculated values are also shown in Fig. 3(c) and are seen to be in good general agreement with the measured values.

The occurrence of a maximum value of ρ_{nc} at $n = 8$ is consistent with the observed maximum improvement in the value of $\sigma_{n\xi}$ relative to $(\sigma_{nx}^2 + \sigma_{ny}^2)^{1/2}$, as observed in Fig. 3(a). However, it is not consistent with Eq. (10) and the accompanying discussion of the preceding section, which gave reason for expecting ρ_{nc} to increase monotonically with increasing n.

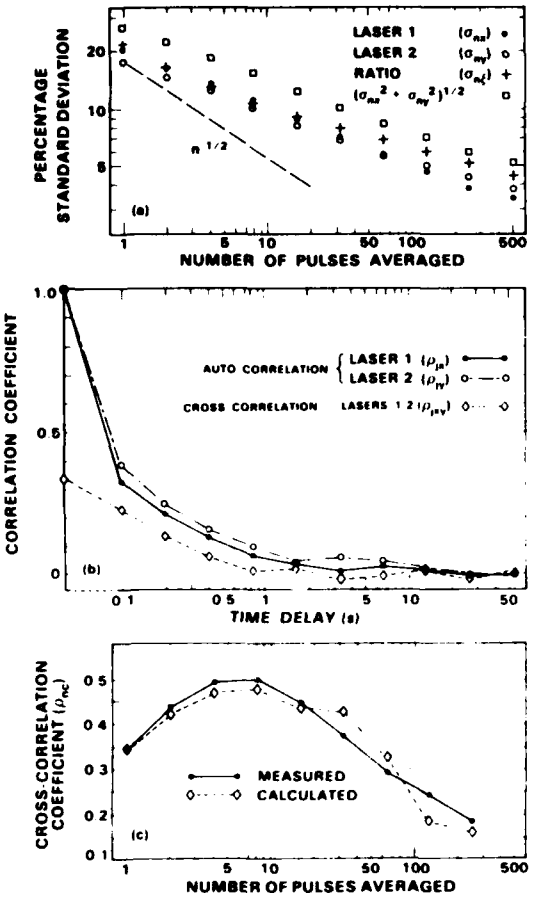

Fig. 3. Lidar signal return data from diffusely reflecting target at a 2.7-km range using direct detection during the period of essentially constant average atmospheric extinction: (a) standard deviation of returns from lasers 1 and 2 and their ratio as functions of the number of pulses averaged; (b) temporal autocorrelation and cross correlation of laser return signals as functions of time delay; and (c) comparison of measured and calculated value of signal-averaged cross-correlation coefficient as a function of the number of pulses averaged.

To explain this apparent contradiction it should be noted that the deivation of Eq. (9) assumed $\rho_{jx} = \rho_{jy}$. As seen in Fig. 3(b) this is not strictly accurate; more important, it can be observed that there is a significant amount of scatter or noise in the correlation function data. This scatter in ρ_{ji}, denoted ϵ_{ji} ($i = 1,2,3 = x,y,xy$, respectively), appears to be of the order of ± 0.02 and is at least as large as ρ_{jxy} as for ρ_{jx} and ρ_{jy}. When the value of the correlation functions decreases to values comparable with or smaller than ϵ_{ji}, which occurs of the order of 1 sec for the data shown in Fig. 3(b), the apparent effect is to bias the ratio,

$$(\rho_{jxy} + \epsilon_{jxy})/[(\rho_{jx} + \epsilon_{jx})^{1/2}(\rho_{jy} + \epsilon_{jy})^{1/2}],$$

toward a smaller value relative to that for $\epsilon = 0$. While the reason for this is not fully understood, it is believed to be due to the increased probability of obtaining a negative value for delay times corresponding to j values for which $\rho_{ji} < \epsilon_{ji}$. For the case of varying atmospheric extinction this was not observed, since, as seen in Fig. 2(b), $\rho_{ji} > \epsilon_{ji}$ over the entire range of delay times considered (to ~3 min). Hence the expected monotonic increase of ρ_{nc} with increasing n was observed for that case. It is improbable that the observed maximum is an experimental artifact since similar results have been obtained in several experiments performed at different times and under differing conditions.

3. Joint considerations. Although significant differences in the behavior of the measured parameters due to the presence or absence of atmospheric drift are observed in the two experiments, there are noteworthy features common to both experiments.

First, agreement between the measured and calculated values of ρ_{nc} vs n is obtained in both experiments. That this agreement exists despite the different functional dependence on n in the two cases represents a strong validation of Eq. (8) and of the assumptions made in its derivation, as given in Appendix A. Second, the relationship among σ_{nx}, σ_{ny}, $\sigma_{n\xi}$, and ρ_{nc} is accurately described by Eq. (5) for both sets of experiments. This indicates that Eq. (5) is valid for $\sigma_{nx} \approx \sigma_{ny} < 0.2$. The subject of the validity of Eq. (5) for larger values of σ_{nx} and σ_{ny} will be addressed more fully below.

Finally, and perhaps most important, it should be noted that the effect of using a dual laser in combination with the signal averaging process yielded comparable values of $\sigma_{n\xi}$ in both cases. For the case in which the extinction coefficient remains constant, the temporal correlation of the individual laser returns more rapidly approached zero, the improvement due to the ρ_{nc} term is relatively small, and the decreasing values of $\sigma_{n\xi}$ with increasing n are dominated by the effect of signal averaging on the individual returns. This is not true when the atmospheric extinction slowly changes during the experimental period. In that case, as seen in Fig. 2(a), the effectiveness of signal averaging in decreasing the standard deviation of the mean of the individual laser return signals is severely reduced. However, this is accompanied by positive long-term cross correlation, which results in the increasing value of ρ_{nc} with increasing n shown in Fig. 2(c) and which effectively cancels the effect of atmospheric drift on the signal-averaged ratio of the returns, in accord with Eq. (8). A dual-laser system capable of obtaining signal-averaged ratio values may, therefore, play an extremely valuable role in a direct-detection DIAL system studying reflections from a diffusely reflecting target. Its use can result in a 30–50% advantage when the atmosphere is essentially constant during a measurement. More important, it effectively overcomes the much greater measurement uncertainty that can occur in a slowly changing atmospheric environment.

2. *Large Standard Deviation and Large Cross Correlation*

It has been observed that the standard deviation of the backscattered radiation σ is always large (>1) when a heterodyne detection system is used.[15] The corresponding cross-correlation coefficient ρ_c is large when the lidar signals are backscattered from a specular target. However, for heterodyne detection and a diffusely reflecting target, ρ_c is large (>0.9) only when the ra-

diation frequencies ν and ν' from the two lasers are the same. When $\nu \neq \nu'$, ρ_c falls off rapidly, and it is found that $\rho_c < 0.05$ for frequency separations as small as 2 cm^{-1}, the separation between adjacent CO_2 laser lines. This loss of cross correlation is due to the surface roughness of the target, which gives rise to different speckle patterns for the two laser beams when $\nu \neq \nu'$. The relationship of cross correlation with surface roughness and wavelength is given by[30] $\rho_c = \exp\{-[\sqrt{2\pi}\sigma_z(\nu - \nu')]^2\}$, where σ_z is the standard deviation of the surface roughness. We find $\rho_c < 0.05$ for $(\nu - \nu') \sim 2\ cm^{-1}$, which indicates $\sigma_z > 2$ mm. The case where $\nu \neq \nu'$ will be discussed in the following section.

As an example of results for large standard deviation ($\sigma \sim 1.0$) and large cross correlation ($\rho_c > 0.9$), we will consider measurements made of the backscattered radiation from a diffusely reflecting target at a range of 2.7 km, with detection in the heterodyne mode and both lasers of the dual-laser system radiating on the 10.6-μm $P(20)$ CO_2 laser line; i.e., $\nu = \nu'$. Under these conditions, σ_x and σ_y were slightly greater than unity and $\rho_c \approx 0.96$.

The values obtained for σ_{nx}, σ_{ny}, and $\sigma_{n\xi}$ as functions of n for these experimental conditions are given in Fig. 4(a). The results are seen to differ sharply from those given in Figs. 2(a) and 3(a). The reduction of σ_{nx} and σ_{ny} with increasing n is considerably slower than $n^{-1/2}$. However, the high cross-correlation coefficient results in a sharp reduction of the normalized standard deviation of the pulse ratio σ_ξ to 0.58. Furthermore, it is seen that the reduction of $\sigma_{n\xi}$ with increasing n is initially more rapid than $n^{-1/2}$ when one properly averages each set of backscattered lidar returns over n pulses prior to taking their ratio. This remarkable result may result from a combination of three factors: (1) small temporal autocorrelation of pulse-pair ratio; (2) increasing cross-correlation coefficient ρ_{nc} with increasing n; and (3) loss of validity of Eq. (5) for large σ_{nx} and σ_{ny}. These factors are considered in greater detail in the following subsections.

1. Temporal autocorrelation of pulse-pair ratio. The high cross correlation between lasers 1 and 2 results in a strongly reduced value of the temporal autocorrelation of the ratio of the pulse pairs ($n = 1$) from the two lasers $\rho_{j(x/y)}$ relative to those of the individual lasers, ρ_{jx} and ρ_{jy}, for short delay times. This is seen in Fig. 4(b), which gives ρ_{jx}, ρ_{jy}, and $\rho_{j(x/y)}$ as functions of delay time ($j\tau$) for $j = 1,2,4,8,\ldots,512$. This small pulse-pair autocorrelation factor alone is sufficient to give rise to a standard deviation for the ratio which initially decreases almost as $n^{-1/2}$, as seen from the curve labeled ratio first, then averaged in Fig. 4(a). As noted previously, taking the ratio of the individual pulses prior to averaging over the n pulses biases the result. For the case of high cross correlation, the bias is relatively small, but, as seen in Fig. 4(a), its effect is highly significant.

2. Cross-correlation effect. When one properly averages the lidar returns from the individual lasers over the n pulses prior to taking their ratio, one finds that the

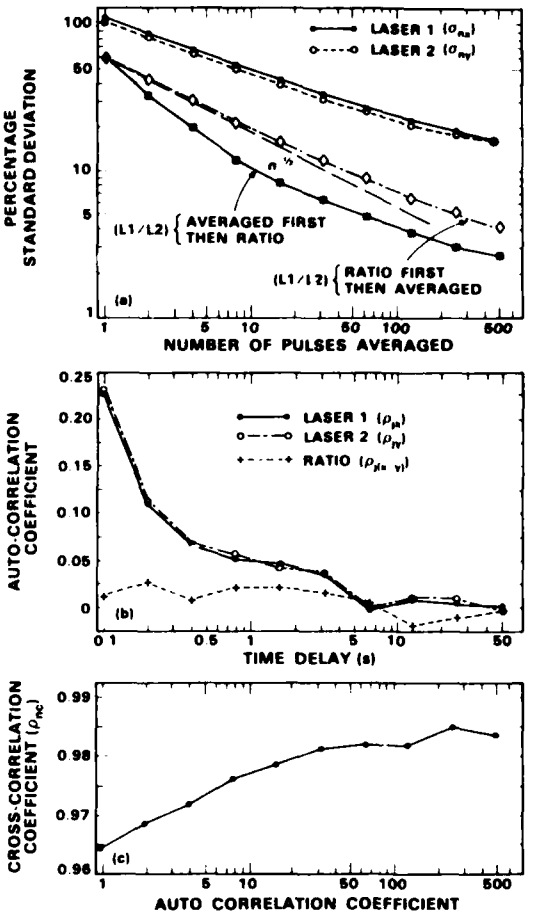

Fig. 4. Lidar signal return data from diffusely reflecting target at a 2.7-km range using heterodyne detection with both CO_2 lasers radiating on the 10.6-μm $P(20)$ laser transition ($\lambda = \lambda'$): (a) Standard deviation of returns from lasers 1 and 2 and their ratio as functions of the number of pulses averaged, showing the $> n^{-1/2}$ variation for small n when the signals are properly averaged prior to taking ratios; (b) temporal autocorrelation of individual laser return signals and of their ratio as functions of time delay; and (c) measured signal-averaged cross-correlation coefficient variation with number of pulses averaged showing the near approach to unity with increasing n.

cross-correlation coefficient ρ_{nc}, as defined by Eq. (9), increases with increasing n, resulting in a further decrease of $\sigma_{n\xi}$ with increasing n. This is shown in Fig. 4(c) where ρ_{nc} is seen to increase from 0.964 for $n = 1$ to $\rho_{nc} > 0.98$ for $n > 16$.

A proportionately greater increase in ρ_{nc} with increasing n, at least initially, was observed under the direct detection of experimental conditions discussed previously, with less dramatic effect on $\sigma_{n\xi}$. The greater effect on $\sigma_{n\xi}$ observed in this case is due to the closeness of ρ_{nc} to unity. This can be seen rather simply by considering the case where $\sigma_{nx} = \sigma_{ny}$. Then from Eq. (5) $\sigma_{n\xi} = \sigma_{ny}\sqrt{2}(1 - \rho_{nc})^{1/2}$ and

$$\frac{d\sigma_{n\xi}}{d\rho_{nc}} = -\frac{\sigma_{ny}/\sqrt{2}}{(1 - \rho_{nc})^{1/2}}. \tag{11}$$

As seen from Eq. (11) the decrease of $\sigma_{n\xi}$ with increasing ρ_{nc} increases dramatically when ρ_{nc} approaches unity.

3. Validity Limit of Eq. (5). As noted previously, the derivation of Eqs. (3) and (5) involved a first-order Taylor series expansion, and the validity of these equations is, therefore, limited to cases where the higher-order terms can be ignored. It is shown in Appendix B that this requires $\sigma_{ny}^2 \ll 1$.

Since all the terms in Eq. (3) have been measured independently, it is possible to make a direct experimental comparison between the measured value $\sigma_{n\xi}$(meas) and $\sigma_{n\xi}$(calc) as calculated on the basis of Eq. (5). The results are shown in Fig. 5 along with σ_{ny}. It is seen that for small n, where σ_{ny} is large, $\sigma_{n\xi}$(meas) is significantly greater than the value predicted by Eq. (5). With increasing n (and decreasing σ_{ny}), $\sigma_{n\xi}$(meas) decreases rapidly and approaches the calculated value. For $n = 8$, where $\sigma_{n\xi} = 0.5$, $\sigma_{n\xi}$(meas) $\approx \sigma_{n\xi}$(calc, and for $n > 8$, the measured value of $\sigma_{n\xi}$ remains in close agreement with the value predicted by Eq. (6). This result indicates that Eq. (5) represents a good approximation for $\sigma_{ny}^2 < 0.25$.

In general, we have always observed $\sigma_{n\xi}$(meas) $\gg$ $\sigma_{n\xi}$(calc) when $\sigma_{ny} \gg 0.5$. In the signal averaging process, this large a value of σ_{ny} has generally been limited to small values of n in our experiments (i.e., to $n < 8$ for the example in Fig. 4(a)]. Therefore, in this region of small n, there may be a relatively rapid decrease in the measured value of $\sigma_{n\xi}$ with increasing n as the value goes from $\sigma_{n\xi}$(meas) $\gg$ $\sigma_{n\xi}$(calc) for $n =$ 1 to $\sigma_{n\xi}$(meas) $\approx$ $\sigma_{n\xi}$(calc) for $n = 8$. Indeed, in Figs. 4(a) and (5), the region where $\sigma_{n\xi}$(meas) decreases with increasing n more rapidly than $n^{-1/2}$ is limited to $n <$ 8. Furthermore, it should be noted that $\sigma_{n\xi}$(calc) varies everywhere more slowly than $n^{-1/2}$.

3. *Large Standard Deviation and Small Cross Correlation*

As noted above, the cross correlation is extremely small for heterodyne detection and backscatter from a diffusely reflecting target when the two lasers are operating at different frequencies. For frequency differences, $\nu - \nu'$, as small as 2 cm^{-1}, ρ_c is typically near zero (<0.05). The value of ρ_{nc} tends to increase slowly with increasing n, but even after averaging over 512 pulses ρ_{nc} values of $\sim 0.25 \pm 0.1$ are typical. Since differential absorption experiments require $\nu \neq \nu'$, this small cross correlation represents a serious limitation to the effectiveness of using lidar backscatter ratios for reducing the effective standard deviation of heterodyne DIAL measurements.

In addition, the combination of large fluctuations and near-zero cross correlation between the lidar returns at the two frequencies leads to a strong bias in their ratio and a large excess variance. As a result, the measured standard deviation of the averaged ratio initially (for small n) is greater than would be obtained by simply considering the standard deviation of the individual sets of lidar returns with zero cross correlation, i.e., $\sigma_{n\xi} > (\sigma_{nx}^2 + \sigma_{ny}^2)^{1/2}$.

This is shown in Fig. 6, which gives the values of $\sigma_{n\xi}$(meas), $\sigma_{n\xi}$(calc), $(\sigma_{nx}^2 + \sigma_{ny}^2)^{1/2}$, σ_{nx}, and σ_{ny}, all as functions of n, obtained experimentally with heterodyne detection of backscattered lidar signals from a diffusely reflecting target with $\nu \neq \nu'$. Specifically, for the results shown in Fig. 6, a flame-sprayed aluminum plate at a 2.7-km range was used as the diffusely reflecting target, with lasers 1 and 2 operating on the 10.6-μm $P(20)$ and $P(22)$ CO_2 laser transitions, respectively. For these lines, $\nu - \nu' = 1.8\,cm^{-1}$. From the figure, it can be seen that use of backscattered signal ratios has some limited value in reducing measurement uncertainty at the larger n values considered but exacts a significant penalty at small n because of the bias effect. It should be noted that the results shown are consistent with the conclusions reached in the preceding section regarding the limits of the validity of Eq. (5).

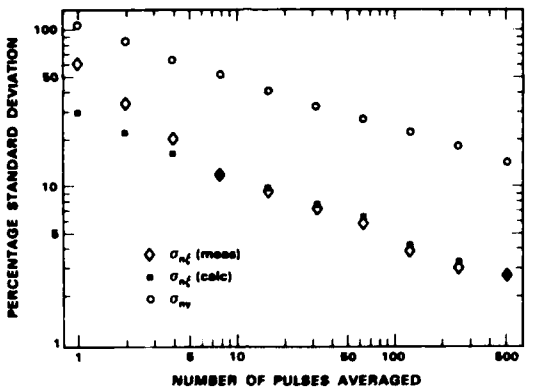

Fig. 5. Comparison of measured and calculated values of $\sigma_{n\xi}$ as a function of the number of pulses averaged based on the data used in Fig. 4. Agreement is seen to be excellent for $\sigma_{ny} \leq 0.5$.

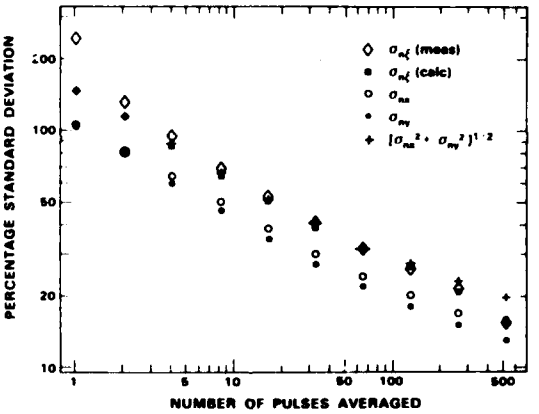

Fig. 6. Standard deviation as functions of the number of pulses averaged for lidar signal returns from the diffusely reflecting target at a 2.7-km range using heterodyne detection with lasers 1 and 2 radiating on the $P(20)$ and $P(22)$ CO_2 laser transitions of the 10.6-μm band, respectively ($\lambda \neq \lambda'$).

V. Conclusions

The previously derived relationships expressed by Eqs. (3) and (4) have been extended to encompass the effects of both signal averaging and cross correlation on the variance of the ratio of averaged backscattered signals from the two lasers of a dual-laser DIAL system.

This extension involved deriving the relationship of the signal-averaged cross-correlation coefficient with the temporal autocorrelation and cross correlation of the individual pulses.

Extensive experimental results using both heterodyne and direct-detection CO_2 lidar measurements were presented and shown to be consistent with the derived relationships. The DIAL experiments investigated the effectiveness of using the ratio of signal returns from a dual-laser system in conjunction with signal averaging in improving measurement accuracy. In general, significant improvement was obtained through such a combination of signal averaging and then taking ratios. However, the degree of improvement was strongly dependent on the relative values of the standard deviation of the lidar signals and the temporal cross correlation.

Specifically, with diffuse targets and direct detection ($\sigma_{n\xi}$ and ρ_{nc} small), improvement due to cross correlation was slight when the atmospheric extinction was essentially constant throughout the measurement period; therefore, under these conditions, use of a dual-laser system does not offer significant improvement in DIAL measurement accuracy. However, when the atmospheric extinction is slowly but constantly varying during the measurement period, use of ratios with a dual-laser system effectively eliminates this variation as a major source of error.

For heterodyne detection of returns from a diffusely reflecting target it was found that both the cross-correlation and the standard deviation are initially large when, and only when, $\nu = \nu'$. On signal averaging, $\sigma_{n\xi}$ decreases with increasing n while ρ_{nc} remains large or increases. Under these conditions, the combination of signal averaging and then taking ratios was shown to be most effective with an initial decrease of $\sigma_{n\xi}$ more rapid than $n^{-1/2}$ possible. On the other hand, for heterodyne detection with backscatter from a diffusely reflecting target and $\nu \neq \nu'$, ρ_c is small, and the standard deviation of the individual laser returns is large. This is the condition for maximum biasing of the ratio and results in a measured value of σ_ξ which is greater than would be obtained by considering the lidar signal returns of the individual lasers. Therefore, use of heteodyne detection in a differential absorption measurement requires signal averaging over a large number of pulses ($n > 10$) at each wavelength prior to taking the ratio to avoid having this bias effect introduce excess error. However, even after signal averaging, the effective cross correlation ρ_{nc} remains small, and, therefore, use of a dual-laser system was found to be of limited value under these experimental conditions.

In addition, the limits of validity of Eqs. (3) and (5) were investigated by carrying out a Taylor series expansion of the ratio to the second order. It was found that higher-order terms, which were ignored in deriving the relationship, could make a significant contribution for large values of $\sigma^2_{n\xi}$. This agreed with experimentally observed differences between $\sigma^2_{n\xi}$(meas) and $\sigma^2_{n\xi}$(calc) for $\sigma^2_{n\xi} > 0.25$, where $\sigma^2_{n\xi}$(calc) was determined on the basis of Eq. (5). However, for $\sigma^2_{n\xi} < 0.25$, generally good agreement between the experimental and calculated values of $\sigma^2_{n\xi}$ was obtained.

The Lincoln Laboratory portion of this work was supported by the National Aeronautical and Space Administration and the Air Force Engineering and Services Center. The University of Maryland portion of this work was supported by the Department of Energy.

Appendix A

To derive Eqs. (5)–(7), which describe the effect of signal averaging on cross correlation and on the variance of the lidar return ratios, several quantities must be defined. We first define $I_{kx} = I_x(t_k)$ and $I_{ky} = I_y(t_k + \Delta t)$ as the normalized deviation of the kth lidar pulse return signals, P_{kx} and P_{ky}, occurring at times t_k and $t_k + \Delta t$, respectively, from their mean values $\bar{P}_x$ and $\bar{P}_y$; i.e.,

$$I_{kx} = (P_{kx} - \bar{P}_x)/\bar{P}_x \text{ and } I_{ky} = (P_{ky} - \bar{P}_y)/\bar{P}_y, \tag{A1}$$

where, as in Eq. (3), subscripts x and y refer to lasers 1 and 2, respectively. The normalized variance of the full set of pulses from laser 1 is then defined as

$$\sigma_x^2 = \langle (I_{kx})^2 \rangle = \frac{1}{\Gamma} \sum_{k=1}^{\Gamma} I_{kx}^2, \tag{A2}$$

where Γ is the total number of pulses from each laser in the data set. ($\Gamma = 6144$ in most experiments described in this paper.) The corresponding temporal autocorrelation coefficient is given by

$$\rho_{jx} = \frac{1}{\sigma_x^2} \langle I_x(t_k) I_x(t_k + j\tau) \rangle$$

$$= \frac{1}{\sigma_x^2 (\Gamma - j)} \sum_{k=1}^{\Gamma - j} I_{kx} I_{(k+j)x}, \tag{A3}$$

where τ is the time interval between pulses from the individual laser. The definitions of the variance and temporal autocorrelation coefficients for laser 2, σ_y^2 and ρ_{jy}, are essentially the same as those given in Eqs. (A2) and (A3) with $x \to y$. The pulse-pair cross-correlation coefficient ρ_c is defined as the covariance of the paired lidar returns from lasers 1 and 2 normalized to their standard deviation; that is,

$$\rho_c = \frac{\sigma_{xy}}{\sigma_x \sigma_y} = \frac{\langle I_x(t_k) I_y(t_k + \Delta t) \rangle}{\sigma_x \sigma_y}$$

$$= \frac{1}{\sigma_x \sigma_y \Gamma} \sum_{k=1}^{\Gamma} I_{kx} I_{ky} \tag{A4}$$

When considering temporal cross correlation for delay times of the order of $j\tau$ (i.e., $j\tau \pm \Delta t$ where $\Delta t \ll j\tau$), one has

$$\rho_{jxy} = \frac{\langle I_x(t_k) I_y(t_k + \Delta t + j\tau) \rangle}{\sigma_x \sigma_y}$$

$$= \frac{1}{\sigma_x \sigma_y (\Gamma - j)} \sum_{k=1}^{\Gamma - j} I_{kx} I_{(k+j)y} \tag{A5}$$

Using the above definitions, one may evaluate the variance and the cross correlation of the Γ lidar returns from both lasers after they have been averaged over n returns. This calculation has already been carried out

for the variance of the individual lasers in Ref. 19, where it was shown that

$$\sigma_{ni}^2 = (\sigma_i^2/n)\left[1 + 2\sum_{j=1}^{n-1}(1 - j/n)\rho_{ji}\right], \tag{A6}$$

where $i = x,y$.

The corresponding averaged cross-correlation coefficient is given by

$$\rho_{nc} = \frac{1}{\sigma_{nx}\sigma_{ny}}\left[\frac{1}{\Gamma/n}\left(\left(\frac{I_{1x} + I_{2x} + \ldots + I_{nx}}{n}\right)\left(\frac{I_{1y} + I_{2y} + \ldots + I_{ny}}{n}\right)\right.\right.$$
$$+ \left(\frac{I_{(n+1)x} + \ldots + I_{2nx}}{n}\right)\left(\frac{I_{(n+1)y} + \ldots + I_{2ny}}{n}\right) + \ldots$$
$$\left.\left. + \left(\frac{I_{\lfloor\Gamma-(n-1)\rfloor x} + \ldots + I_{\Gamma x}}{n}\right)\left(\frac{I_{\lfloor\Gamma-(n-1)\rfloor y} + \ldots + I_{\Gamma y}}{n}\right)\right)\right] \tag{A7}$$

$$= \frac{1}{n\Gamma\sigma_{nx}\sigma_{ny}}\left[(I_{1x}I_{1y} + I_{2x}I_{2y} + \ldots + I_{\Gamma x}I_{\Gamma y})\right.$$
$$+ (\lfloor I_{1x}I_{2y} + \ldots + I_{(n-1)x}I_{ny}\rfloor + \lfloor I_{2x}I_{1y} + \ldots + I_{nx}I_{(n-1)y}\rfloor$$
$$+ \lfloor I_{(n+1)x}I_{(n+2)y} + \ldots + I_{(2n-1)x}I_{2ny}\rfloor$$
$$+ \lfloor I_{(n+2)x}I_{(n+1)y} + \ldots + I_{2nx}I_{(2n-1)y}\rfloor + \ldots$$
$$+ \lfloor I_{\lfloor\Gamma-(n-1)\rfloor x}I_{\lfloor\Gamma-(n-2)y\rfloor} + \ldots + I_{(\Gamma-1)x}I_{\Gamma y}\rfloor$$
$$+ \lfloor I_{\lfloor\Gamma-(n-1)y\rfloor}I_{\lfloor\Gamma-(n-2)x\rfloor} + \ldots + I_{\Gamma x}I_{(\Gamma-1)y}\rfloor)$$
$$+ \ldots + (\lfloor I_{1x}I_{ny} + I_{(n+1)x}I_{2ny} + \ldots + I_{\lfloor\Gamma-(n-1)\rfloor x}I_{\Gamma y}\rfloor$$
$$\left. + \lfloor I_{nx}I_{1y} + I_{2nx}I_{(n+1)y} + \ldots + I_{\Gamma x}I_{\lfloor\Gamma-(n-1)\rfloor y}\rfloor)\right]. \tag{A8}$$

The terms within the first bold parentheses of Eq. (A8) can be broken into pairs which refer to the same subset of n pulses; i.e., $k = 1$ to n, $n + 1$ to $2n$, $\ldots$ $\Gamma - (n - 1)$ to Γ, as shown. The time delay differs in the two terms of such a pair in that the delay will be $(j\tau + \Delta t)$ for one term and $(j\tau - \Delta t)$ for the other term. In our experiments, $j\tau$ is some multiple of 100 msec, while $\Delta t \approx 5$–10 μsec. The atmosphere can be considered frozen over the time delay difference $2\Delta t$, and this difference can, therefore, be ignored. In addition, since both I_{kx} and I_{ky} are normalized, one may, as a reasonable approximation, assume that when averaged over the full set, $I_{kx}I_{(k+j)y} \approx I_{(k+j)x}I_{ky}$. In that case, the two terms dealing with the same pulse subset may be considered equivalent, and from Eqs. (A4) and (A5)

$$\rho_{nc} = \frac{1}{n\Gamma\sigma_{nx}\sigma_{ny}}\left\{\Gamma\rho_c\sigma_x\sigma_y + 2(\Gamma - 1)\sigma_x\sigma_y\left(\frac{n-1}{n}\right)\rho_{1xy} + \ldots\right.$$
$$\left. + 2\lfloor\Gamma - (n-1)\rfloor\sigma_x\sigma_y\left(\frac{1}{n}\right)\rho_{(n-1)xy}\right\}. \tag{A9}$$

or

$$\rho_{nc} = \frac{\sigma_x\sigma_y}{n\sigma_{nx}\sigma_{ny}}\left[\rho_c + 2\sum_{j=1}^{n-1}(1 - j/\Gamma)(1 - j/n)\rho_{jxy}\right]. \tag{A10}$$

Equations (A9) and (A10) assume equal weighting of interpolated missing terms in Eq. (A8), as discussed in Ref. 19. The derivation of Eq. (A10) closely parallels the derivation of σ_n^2 given there for the segmentally averaged case. It was shown that for a sufficiently large sample, the $(1 - j/\Gamma)$ term ≈ 1, and Eq. (A10) effectively reduces to the form

$$\rho_{nc} = \frac{\sigma_x\sigma_y}{n\sigma_{nx}\sigma_{ny}}\left[\rho_c + 2\sum_{j=1}^{n-1}(1 - j/n)\rho_{jxy}\right]. \tag{A11}$$

In a similar fashion, one may use the approach described in Appendix C of Ref. 19 to show that Eq. (A11) is obtained directly when a running average rather than a segmental average is used to define the mean value of the n pulses being integrated.

Appendix B: Calculation of Variance of $\xi(=x/y)$ to Second Order

In general, the Taylor expansion of a function z of two variables, x and y, evaluated at a point p corresponding to the averaged values, $\bar{x}$ and $\bar{y}$, is given to second order in the derivatives by

$$z = f(x,y) = f(\bar{x},\bar{y})$$
$$+ \left.\frac{\partial f}{\partial x}\right|_p (x - \bar{x}) + \left.\frac{\partial f}{\partial y}\right|_p (y - \bar{y})$$
$$+ \frac{1}{2}\left[\left.\frac{\partial^2 f}{\partial x^2}\right|_p (x - \bar{x})^2\right.$$
$$\left. + \left.\frac{\partial^2 f}{\partial y^2}\right|_p (y - \bar{y})^2 + 2\left.\frac{\partial^2 f}{\partial x\partial y}\right|_p (x - \bar{x})(y - \bar{y})\right], \tag{B1}$$

while the average value $\bar{z}$ is

$$\bar{z} = f(\bar{x},\bar{y}) + \frac{1}{2}\left\{\left.\frac{\partial^2 f}{\partial x^2}\right|_p \langle(x - \bar{x})^2\rangle\right.$$
$$\left. + \left.\frac{\partial^2 f}{\partial y^2}\right|_p \langle(y - \bar{y})^2\rangle + 2\left.\frac{\partial^2 f}{\partial_x\partial_y}\right|_p \langle(x - \bar{x})(y - \bar{y})\rangle\right\}$$
$$= f(\bar{x},\bar{y}) + \frac{1}{2}\left(\left.\frac{\partial^2 f}{\partial x^2}\right|_p \sigma_x^2 + \left.\frac{\partial^2 f}{\partial y^2}\right|_p \sigma_y^2 + 2\left.\frac{\partial^2 f}{\partial x\partial y}\right|_p \rho_c\sigma_x\sigma_y\right). \tag{B2}$$

The variance of z may be given by

$$\sigma_z^2 = \langle(z - \bar{z})^2\rangle = \left\langle\left(\frac{\partial f}{\partial x}\right)^2 (x - \bar{x})^2 + \left(\frac{\partial f}{\partial y}\right)^2 (y - \bar{y})^2\right.$$
$$+ 2\left(\frac{\partial f}{\partial x}\right)\left(\frac{\partial f}{\partial y}\right)(x - \bar{x})(y - \bar{y}) + \left\{\frac{\partial f}{\partial x}\left(\frac{\partial^2 f}{\partial x^2}\right)(x - \bar{x})^3\right.$$
$$+ \left[2\left(\frac{\partial f}{\partial x}\right)\left(\frac{\partial^2 f}{\partial x\partial y}\right) + \frac{\partial f}{\partial y}\left(\frac{\partial^2 f}{\partial x^2}\right)\right](x - \bar{x})^2(y - \bar{y})$$
$$+ \left[2\left(\frac{\partial f}{\partial y}\right)\left(\frac{\partial^2 f}{\partial y\partial x}\right) + \frac{\partial f}{\partial x}\left(\frac{\partial^2 f}{\partial y^2}\right)\right](x - \bar{x})(y - \bar{y})^2$$
$$\left. + \frac{\partial f}{\partial y}\left(\frac{\partial^2 f}{\partial y^2}\right)(y - \bar{y})^3\right\}$$
$$+ \frac{1}{4}\left\{\left(\frac{\partial^2 f}{\partial x^2}\right)^2 [(x - \bar{x})^4 - \sigma_x^4]\right.$$
$$+ 4\left(\frac{\partial^2 f}{\partial x^2}\right)\left(\frac{\partial^2 f}{\partial x\partial y}\right)[(x - \bar{x})^3(y - \bar{y}) - \rho_c\sigma_x^3\sigma_y]$$
$$+ 4\left(\frac{\partial^2 f}{\partial x\partial y}\right)^2 [(x - \bar{x})^2(y - \bar{y})^2 - \rho_c\sigma_x^2\sigma_y^2]$$
$$+ 2\left(\frac{\partial^2 f}{\partial x^2}\right)\left(\frac{\partial^2 f}{\partial y^2}\right)[(x - \bar{x})^2(y - \bar{y})^2 - \sigma_x^2\sigma_y^2]$$
$$+ 4\left(\frac{\partial^2 f}{\partial y^2}\right)\left(\frac{\partial^2 f}{\partial x\partial y}\right)[(x - \bar{x})(y - \bar{y})^3 - \rho_c\sigma_x\sigma_y^3]$$
$$\left.\left. + \left(\frac{\partial^2 f}{\partial y^2}\right)^2 [(y - \bar{y})^4 - \sigma_y^4]\right\}\right\rangle. \tag{B3}$$

where all the derivatives are evaluated at point $p = x,y$. For $z = \xi = x/y$

$$\left.\frac{\partial f}{\partial x}\right|_p = \frac{1}{\bar{y}}, \left.\frac{\partial^2 f}{\partial x^2}\right|_p = 0, \left.\frac{\partial f}{\partial y}\right|_p = -\frac{\bar{x}}{\bar{y}},$$
$$\left.\frac{\partial^2 f}{\partial y^2}\right|_p = \frac{2\bar{x}}{\bar{y}^3}, \text{ and } \left.\frac{\partial^2 f}{\partial x\partial y}\right|_p = \left.\frac{\partial^2 f}{\partial y\partial x}\right|_p = -\frac{1}{\bar{y}^2}.$$

Substituting into Eq. (B3) and normalizing,

$$\frac{\langle(\xi-\bar{\xi})^2\rangle}{(\bar{x}^2/\bar{y}^2)} = \left\langle\left[\frac{(x-\bar{x})^2}{\bar{x}^2} - \frac{2(x-\bar{x})(y-\bar{y})}{\bar{x}\bar{y}} + \frac{(y-\bar{y})^2}{\bar{y}^2}\right] - 2\left[\frac{(x-\bar{x})^2(y-\bar{y})}{\bar{x}^2\bar{y}} - \frac{2(x-\bar{x})(y-\bar{y})^2}{\bar{x}\bar{y}^2} + \frac{(y-\bar{y})^3}{\bar{y}^2}\right] + \left[\frac{(x-\bar{x})^2(y-\bar{y})^2}{\bar{x}^2\bar{y}^2} - \frac{2(x-\bar{x})(y-\bar{y})^3}{\bar{x}\bar{y}^3} + \frac{(y-\bar{y})^4}{\bar{y}^4}\right] - \sigma_y^2(\sigma_x^2 + \sigma_y^2 - 2\rho_c\sigma_x\sigma_y)\right\rangle . \quad \text{(B4)}$$

In Eq. (B4), σ_x and σ_y represent the normalized standard deviation values. The equation may be rewritten

$$\sigma_\xi^2 = \left\langle\left[1 - \frac{(y-\bar{y})}{\bar{y}}\right]^2\left\{\frac{(x-\bar{x})^2}{\bar{x}^2} + \frac{(y-\bar{y})^2}{\bar{y}^2} - \frac{2(x-\bar{x})(y-\bar{y})}{\bar{x}\bar{y}}\right\} - \sigma_y^2(\sigma_x^2 + \sigma_y^2 - 2\rho_c\sigma_x\sigma_y)\right\rangle . \quad \text{(B5)}$$

The term in braces on the right-hand side of Eq. (B5) is just the solution obtained for the variance of the lidar return of σ_ξ^2 for the first-order Taylor series expansion and as given in Eq. (2). In that equation, σ_y^2 is identified with

$$\frac{\langle(y-\bar{y})^2\rangle}{\bar{y}^2} .$$

It is apparent that, for values of σ_y^2 (or σ_{ny}^2 in the signal averaged case) approaching unity, higher-order terms in the Taylor series expansion play a significant role and cannot be ignored. Therefore, the validity of Eqs. (3) and (5) is limited to the cases where $\sigma_y^2 \ll 1$ or $\sigma_{ny}^2 \ll 1$, respectively. This is consistent with the experimental results given in the paper, which indicate serious discrepancies between measured values of $\sigma_{n\xi}^2$, and values calculated on the basis of Eqs. (3) or (5) occur when $\sigma_{ny}^2 > 0.25$.

Although the moments of each of the third- and fourth-order terms in Eq. (B4) can be calculated when the distribution function of the lidar signals is known, such calculations are beyond the scope of this paper. However, it should be noted that while the third-order terms would be zero for a symmetrical distribution function, lidar return distributions tend to be strongly asymmetric (i.e., lognormal, negative exponential, or k distribution) and dependent on experimental conditions. Therefore, the third-order term must be retained.

It was observed that when the Taylor series expansion is limited to first order, $\sigma_\xi^2 = \sigma_{\ln\xi}^2$.[20] This is not true for higher-order expansions.

References

1. D. K. Killinger and A. Mooradian, Eds., *Optical and Laser Remote Sensing* (Springer, Berlin, 1983).
2. J. H. Shapiro, B. A. Capron, and R. C. Harney, "Imaging and Target Detection with a Heterodyne-Reception Optical Radar," Appl. Opt. **20**, 3292 (1981).
3. P. Brockman, R. V. Hess, L. D. Staton, and C. H. Bair, "DIAL with Heterodyne Detection Including Speckle Noise: Aircraft/Shuttle Measurements of O_3, H_2O and NH_3 with Pulsed Tunable Lasers, NASA Tech. Paper 1725 (1980).
4. R. M. Hardesty, "A Comparison of Heterodyne and Direct Detection CO_2 DIAL Systems for Ground Based Humidity Profiling," NOAA Tech. Memo. ERL WP-64 (1980).
5. R. J. Hill, S. F. Clifford, and R. S. Lawrence, "Refractive-Index and Absorption Fluctuations in the Infrared Caused by Temperature, Humidity, and Pressure Fluctuations," J. Opt. Soc. Am. **70**, 1192 (1980).
6. A. G. Kjelaas, P. E. Nordal, and A. Bjerkestrand, "Scintillation and Multiwavelength Coherence Effects in a Long-Path Laser Absorption Spectrometer," Appl. Opt. **17**, 277 (1978).
7. J. F. Holmes and V. S. Rao Gudimetla, "Variance of Intensity for a Discrete Spectrum, Polychromatic Speckle Field after Propagation Through the Turbulent Atmosphere," J. Opt. Soc. Am. **71**, 1176 (1981).
8. J. W. Goodman, "Some Effects of Target-Induced Scintillation on Optical Radar Performance," Proc. IEEE **53**, 1688 (1965).
9. C. M. McIntyre, M. H. Lee, and J. H. Churnside, "Statistics of Irradiance Scattered from a Diffuse Target Containing Multiple Glints," J. Opt. Soc. Am. **70**, 1084 (1980).
10. T. Chiba, "Spot Dancing of the Laser Beam Propagated Through the Turbulent Atmosphere," Appl. Opt. **10**, 2456 (1971).
11. M. H. Lee and J. F. Holmes, "Effect of the Turbulent Atmosphere on the Autocovariance Function for Speckle Field Generated by a Laser Beam with Random Pointing Error," J. Opt. Soc. Am. **71**, 559 (1981).
12. G. Megie and R. T. Menzies, "Complementarity of UV and IR Differential Absorption Lidar for Global Measurements of Atmospheric Species," Appl. Opt. **19**, 1173 (1980).
13. C. S. Gardner and G. S. Micherle, "Speckle Noise in Direct Detection LIDAR Systems," U. Illinois Radio Research Report 495 (1978).
14. C. S. Gardner and A. M. Saleh, "Speckle Noise in Differential Absorption LIDAR Systems," U. Illinois Radio Research Report 496 (1978).
15. D. K. Killinger, N. Menyuk, and W. E. DeFeo, "Experimental Comparison of Heterodyne and Direct Detection for Pulsed Differential Absorption," Appl. Opt. **22**, 682 (1983).
16. E. Jakeman, C. J. Oliver, and E. R. Pike, "Optical Homodyne Detection," Adv. Phys. **24**, 349 (1975).
17. M. Elbaum and M. C. Teich, "Heterodyne Detection of Random Gaussian Signals in the Optical and Infrared: Optimization of Pulse Duration," Opt. Commun. **27**, 257 (1978).
18. N. Menyuk, D. K. Killinger, and W. E. DeFeo, "Laser Remote Sensing of Hydrazine, MMH, and UDMH Using a Differential Absorption CO_2 Lidar," Appl. Opt. **21**, 2275 (1982).
19. N. Menyuk, D. K. Killinger, and C. R. Menyuk, "Limitations of Signal Averaging due to Temporal Correlation in Laser Remote-Sensing Measurements," Appl. Opt. **21**, 3377 (1982).
20. D. K. Killinger and N. Menyuk, "Effect of Turbulence-Induced Correlation on Laser Remote Sensing Errors," Appl. Phys. Lett. **38**, 968 (1981).
21. For simplicity, Eq. (2) ignores the effect of possible differences in target reflectivity or background absorption at the two frequencies. This omission does not affect later discussions.
22. N. Menyuk and D. K. Killinger, "Temporal Correlation Measurements of Pulsed Dual CO_2 Lidar Returns," Opt. Lett. **6**, 301 (1981).
23. B. Marthinsson, J. Johansson, and S. T. Eng, "Air Pollution Monitoring with a Computer-Controlled CO_2-Laser Long-Path Absorption System," Opt. Quantum Electron. **12**, 327 (1980).
24. R. M. Hardesty, R. J. Keeler, M. J. Post, and R. A. Richter, "Characteristics of Coherent Lidar Returns from Calibration Targets and Aerosols," Appl. Opt. **20**, 3763 (1981).
25. J. L. Bufton, T. Itabe, and D. A. Grolemund, "Dual-Wavelength Correlation Measurements with an Airborne Pulsed Carbon Dioxide Lidar System," Opt. Lett. **7**, 584 (1982).
26. D. K. Killinger, N. Menyuk, and W. E. DeFeo, "Remote Probing

of the Atmosphere Using a CO_2 DIAL System," IEEE J. Quantum Electron. **QE-17**, 1917 (1981).
27. J. F. Holmes, "The Effects of Target Induced Speckle, Atmospheric Turbulence and Beam Pointing Jitter on the Errors in Remote Sensing Measurements," in *Optical and Laser Remote Sensing*, D. K. Killinger and A. Mooradian, Eds. (Springer, Berlin, 1983), pp. 164–169.
28. B. J. Rye, "Power Ratio Estimation in Incoherent Backscatter Lidar: Heterodyne Receiver with Square Law Detection," J. Climate Appl. Meteorol. **22**, 1899 (1983).
29. N. Menyuk and P. F. Moulton, "Development of a High-Repetition-Rate Mini-TEA Laser," Rev. Sci. Instrum. **51**, 216 (1980).
30. J. W. Goodman and G. Parry, in *Laser Speckle and Related Phenomena*, J. C. Dainty, Ed. (Springer, New York, 1975), Chaps. 2 and 3, respectively.

Appendix B

The following is a preprint of a journal article to be published in Applied Optics entitled "Laser Remote Sensing of Atmospheric Ammonia Using a CO_2 LIDAR System."

LASER REMOTE SENSING OF ATMOSPHERIC AMMONIA USING A CO_2 LIDAR SYSTEM*

A. P. Forcet, D. K. Killinger, W. E. DeFeo and N. Menyuk

Lincoln Laboratory, Massachusetts Institute of Technology

Lexington, Massachusetts 02173-0073

Abstract

A CO_2 differential-absorption LIDAR system has been used for the remote sensing of ammonia in the atmosphere. For CO_2 LIDAR returns backscattered from topographic targets at ranges up to 2.7 km, the path-averaged sensitivity of the DIAL system was 5 parts per billion of NH_3. Concentrations of atmospheric ammonia were found to vary during the day from undetectable levels (< 5 ppb) to as high as 20 ppb, depending upon temperature and humidity conditions.

*This work was supported by The National Aeronautical and Space Administration and the Air Force Engineering and Services Center.

†Visiting Scientist from U. S. Army Chemical Research and Development Center, Aberdeen Proving Ground.

LASER REMOTE SENSING OF ATMOSPHERIC AMMONIA USING A CO_2 LIDAR SYSTEM*

A. P. Forcet, D. K. Killinger, W. E. DeFeo and N. Menyuk
Lincoln Laboratory, Massachusetts Institute of Technology
Lexington, Massachusetts 02173-0073

I. Introduction

Single-ended differential-absorption LIDAR (DIAL) has been shown to be a sensitive method for the long-range remote sensing of trace molecular species in the atmosphere. DIAL systems operating in the infrared have been used to monitor several trace atmospheric constituents[1-5] including C_2H_4, NO, SO_2, and O_3 and work is underway to increase the number of atmospheric species which can be detected.

In this paper, the use of a pulsed infrared CO_2-laser DIAL system for the remote sensing of atmospheric NH_3 is reported. For CO_2 LIDAR returns backscattered from targets at a range of 2.7 km, the experiments demonstrate the ability of the DIAL system to remotely sense the presence of NH_3 with a path-averaged detection sensitivity of 5 parts per billion (ppb). The concentration of ambient atmospheric NH_3 was observed to vary between undetectable levels (< 5 ppb) to values as high as 20 ppb. In addition, an apparent negative correlation between the concentration of atmospheric NH_3 and relative humidity or water vapor aerosol concentration was also observed.

Atmospheric ammonia is produced by a combination of natural and anthropogenic sources[6]. Its detection and measurement is important in that its concentration is a critical parameter in the rates of formation, transport,

*This work was supported by The National Aeronautical and Space Administration and the Air Force Engineering and Services Center.
†Visiting Scientist from U. S. Army Chemical Research and Development Center, Aberdeen Proving Ground.

transformation and removal of the sulfur and nitrogen aerosols which play an important role in the generation of acid rain[7]. Previous measurements of atmospheric NH_3 have generally relied on wet-chemical techniques, which require the collection of atmospheric samples[7,8]. The sensitivity of such techniques along with the period of time required for sample collection have limited the time resolution of the measurements to periods of several hours. In contrast, DIAL systems are capable of in situ real-time measurements, and may thus play a significant role in future atmospheric measurements. This paper presents preliminary experiments which indicate the capability of the CO_2 DIAL technique for measurement of atmospheric NH_3 concentrations.

II. Experimental Apparatus

A schematic of the dual-CO_2 laser DIAL system used in our experiments is shown in Fig. 1 and has been described previously.[3,9] The pulsed transmitted radiation was provided by two line-tunable mini-TEA CO_2 lasers. The CO_2 lasers, typically, have a linewidth on the order of 0.1 cm^{-1}, an output energy of 10 mJ/pulse, a pulselength of 100 nsec, and operate at a PRF of 15 Hz.

As seen in Fig. 1, the outputs of the two lasers were collimated and then joined with a 50/50 beam splitter. Portions of each beam were directed to a spectrometer, a pyroelectric detector to normalize the pulse intensities, and through a Pyrex absorption cell (33.5 cm long x 2.54 cm diameter with BaF_2 windows) to calibrate the NH_3 absorption levels. The remainder of the laser radiation was sent through a 10X beam expander and directed to either a topographic target (the wall of a building), a flame-sprayed aluminum plate , or a one-inch retroreflector, all at a range of 2.7 km. Backscattered LIDAR returns

re collected with a 30 cm Cassegrain telescope and focused onto a cooled
CdTe detector ($D^* = 2.8 \times 10^{10}$ cm $Hz^{1/2}$ W^{-1}). The signals from the
tectors were recorded and analyzed by a computer based data acquisition system
ich calculated the normalized differential absorption of the laser radiation
rough the laboratory absorption cell and that of the LIDAR returns. For
libration purposes, a large, chemically-inert, polypropylene tank (104 cm long
52.5 cm diameter with 15° slanted polyethylene windows) could be placed
tside the window in the path of the laser beams to measure the absorption of
e laser radiation for known amounts of NH_3 in the tank; a muffin fan was
aced inside the tank to reduce stratification of NH_3 in the tank.

Normally, for dual-laser DIAL operation Laser 1 was tuned to a transition
equency which had low NH_3 absorption and Laser 2 was tuned to a frequency
ich had high NH_3 absorption; the lasers were separately triggered with a
ne delay of 50-μs in order to freeze the effect of atmosphere turbulence
tween the two output pulses.[9] Under some experimental conditions, however,
ly one laser was used for the DIAL experiments and was sequentially tuned on
l off-resonance; this single-laser DIAL measurement was necessary because one
the lasers in Fig. 1 would not lase on the required transitions for use with
e strongest NH_3 absorption line. The distinction between single and dual-
ser DIAL measurements will be made clear in the discussion of experimental
.a.

. Choice of Laser Frequencies

The choice of CO_2 laser frequencies for the remote sensing of NH_3 is
ermined by several factors. First, the choice of frequencies is limited to

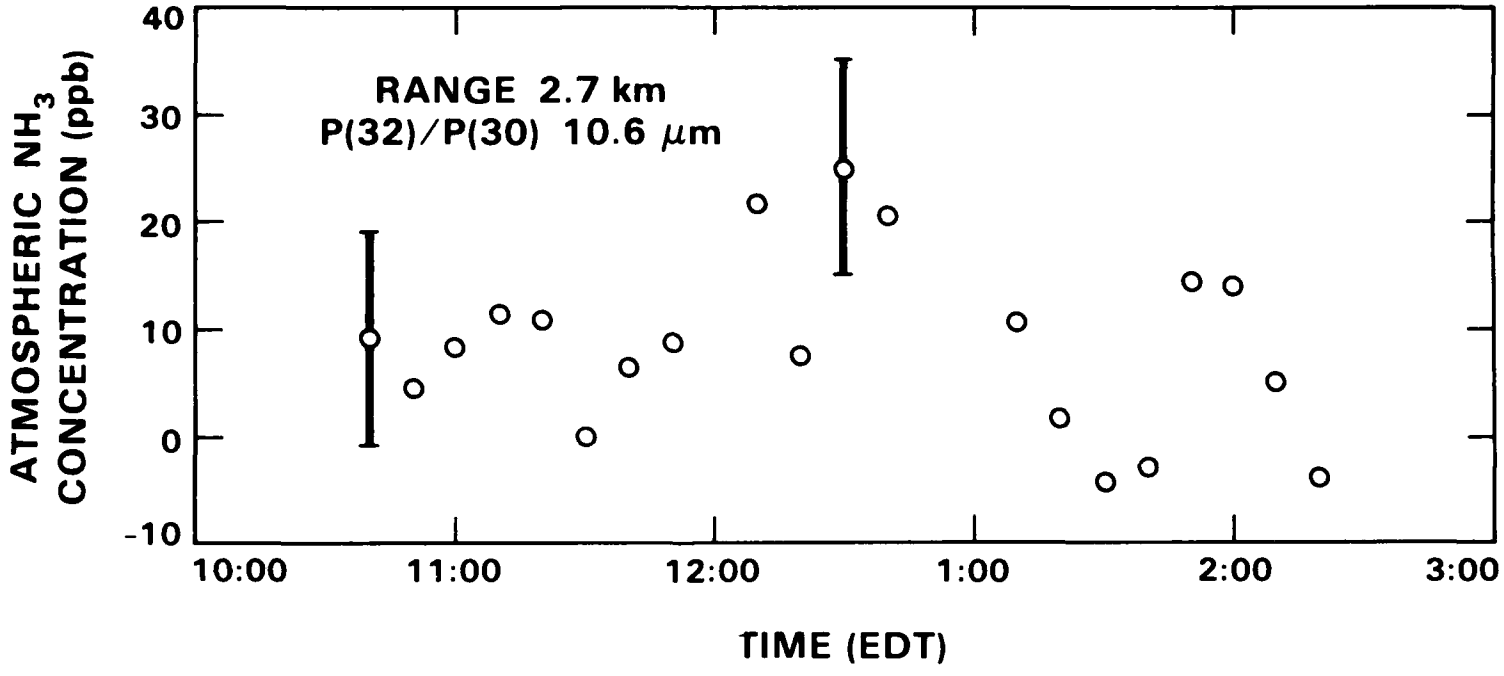
RANGE 2.7 km
P(32)/P(30) 10.6 μm
ATMOSPHERIC NH3 CONCENTRATION (ppb)
40
30
20
10
0
-10
10:00
11:00
12:00
1:00
2:00
3:00
TIME (EDT)

Figure 3.

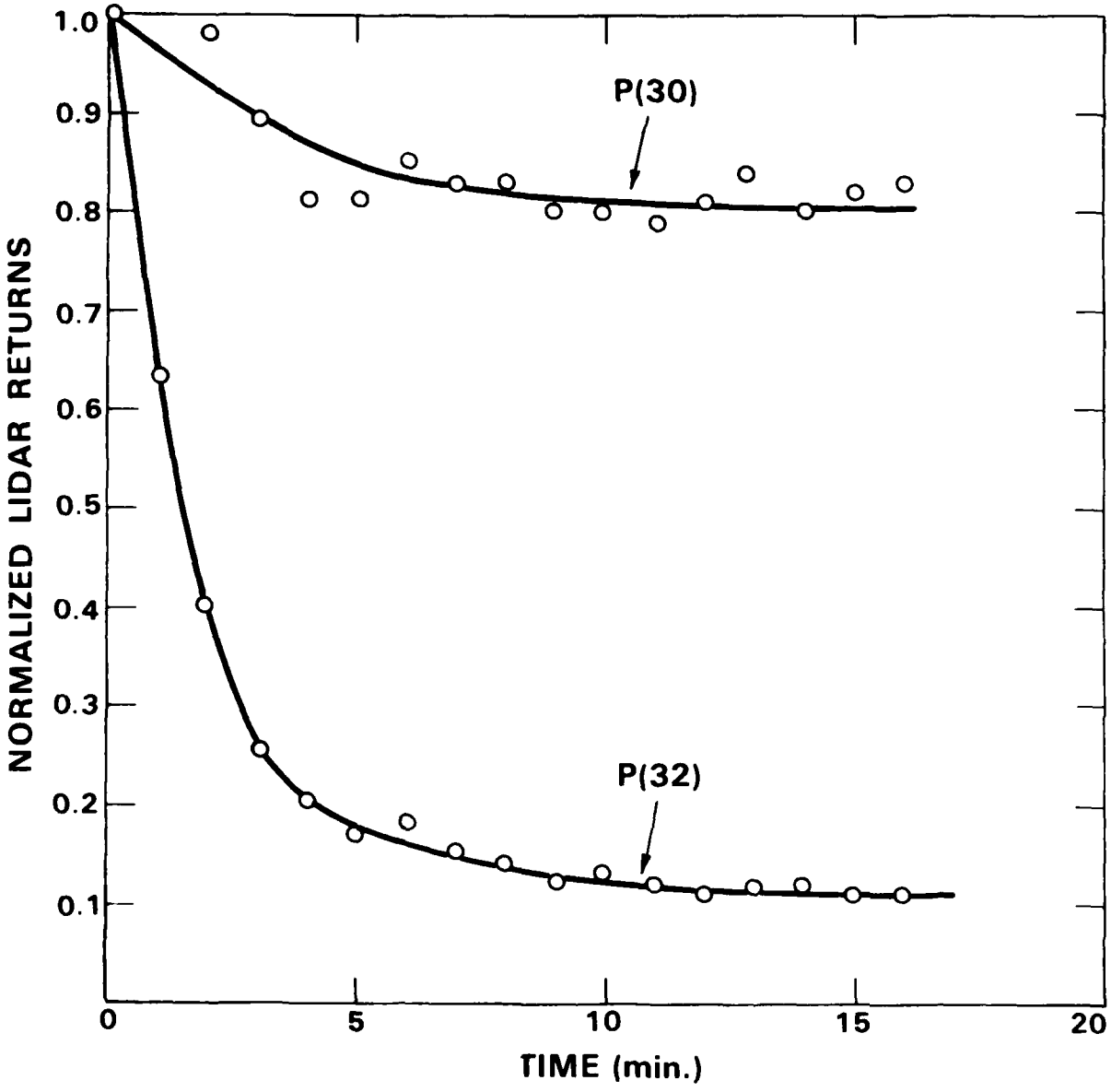
NORMALIZED LIDAR RETURNS
1.0
0.9
0.8
0.7
0.6
0.5
0.4
0.3
0.2
0.1
P(30)
P(32)
0
5
10
15
20
TIME (min.)

Figure 2.

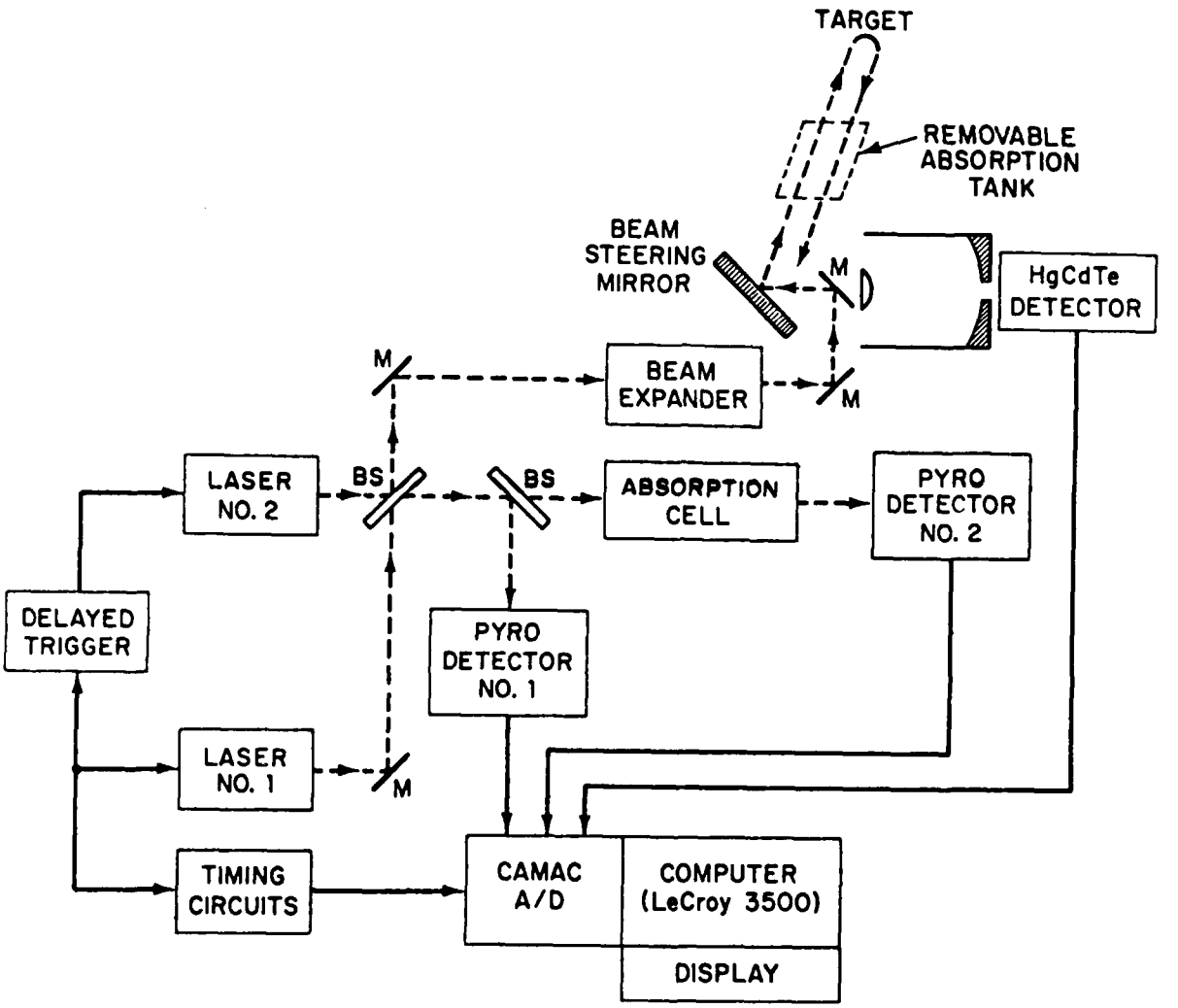
TARGET
REMOVABLE ABSORPTION TANK
BEAM STEERING MIRROR
M
HgCdTe DETECTOR
M
BEAM EXPANDER
M
LASER NO. 2
BS
BS
ABSORPTION CELL
PYRO DETECTOR NO. 2
DELAYED TRIGGER
PYRO DETECTOR NO. 1
LASER NO. 1
M
TIMING CIRCUITS
CAMAC A/D
COMPUTER (LeCroy 3500)
DISPLAY
LRS Final (8-1)

Figure 1.

Table I

CO_2 Laser Line	Wavelength $\lambda(\mu m)$	NH_3 Absorption[A] Coefficient σ $(atm \cdot cm)^{-1}$	Atmospheric[B] Attenuation α km^{-1}	
			Summer	Winter
*R(30)	9.217	56.	.23	.06
*R(26)	9.237	0.1	.25	.07
R(16)	9.291	12.7	.34	.10
R(10)	10.316	0.5	.28	.07
R(8)	10.331	20.	NA	NA
R(6)	10.346	26.	NA	NA
*P(30)	10.693	0.9	.28	.05
*P(32)	10.716	13.7	.27	.05
P(34)	10.738	14.0	.26	.05

A: From References 12 and 13.
B: From Reference 14.
*: On-Resonance and Off-Resonance CO_2 Laser Line pairs chosen for DIAL measurements

FIGURE CAPTIONS

Fig. 1. Schematic of the dual-laser LIDAR system used for the remote sensing of ammonia.

Fig. 2. Time variation of LIDAR returns of 10.69-μm P(30) and 10.71-μm P(32) radiation passing through the tank and reflected from a topographic target at a range of 2.7 km after injecting 0.2 cm^3 of 28% aqueous NH_3.

Fig. 3. Dual laser DIAL measurements of ambient atmospheric NH_3 using the 10.69-μm P(30) and 10.71-μm P(32) CO_2 laser lines over a 2.7 km range with 26% relative humidity.

Fig. 4. Single laser DIAL measurements of ambient atmospheric NH_3 using the 9.24-μm R(26) and 9.22-μm R(30) CO_2 laser lines over a 2.7 km range with 26% relative humidity.

Fig. 5. DIAL measurements of ambient atmospheric NH_3 using the 9.24-μm R(26) and 9.22-μm R(30) CO_2 laser lines over a 2.7 km range showing the effect of a change in relative humidity from 54% to 41%.

12. R. R. Patty, G. M. Russwurm, W. A. McLenny and D. R. Morgan, "CO_2 Laser Absorption Coefficients for Determining Ambient Levels of O_3, NH_3, and C_2H_4", Appl. Opt. 13, 2850 (1974).

13. R. J. Brewer and C. W. Bruce, "Photoacoustic Spectroscopy of NH_3 at the 9-μm and 10μm Co_2 Laser Wavelengths", Appl. Opt. 17, 3746 (1978).

14. R. A. McClatchey, R. W. Fenn, J. E. A. Selby, F. E. Volz and J. S. Garing, "Optical Properties of the Atmosphere (Third Edition)", Report AFCRL-72-0497, Environmental Research Paper No. 411 (1972); R. A. McClatchey and J. E. A. Selby, "Atmospheric Transmittance 7-30μm: Attenuation of CO_2 Laser Radiation," Report AFCRL-72-0611, Environmental Research Paper No. 419 (1972).

15. A. G. Kjelaas, P. E. Nordal and A. Bjerkstrand, "Scintillation and Multi-wavelength Coherence Effects in a Long-Path Laser Absorption Spectrometer", Appl. Opt. 17, 277 (1978).

16. J. G. Hawley, D. D. Powell, D. E. Cooper, "Absorption Coefficient of Ammonia for Laser Remote Sensing of Atmospheric Trace Quantities," paper WC28, OSA Topical Meeting: Optical Remote Sensing of the Atmosphere, Jan. 15-18 (1985).

17. A. Mayer, J. Comera, H. Charpentier and C. Jaussaud, "Absorption Coefficients of Various Pollutant Gases At CO_2 Laser Wavelengths; Application to the Remote Sensing of These Pollutants," Appl. Opt. 17, 391 (1978).

18. H. Israel and G. W. Israel, Trace Elements in the Atmosphere (Ann Arbor Science, Ann Arbor, Michigan, 1974).

19. J. C. Petheram, "Differential Backscatter from the Atmospheric Aerosol: The Implications for IR Differential Absorption LIDAR," Appl. Opt. 20, 3941 (1981).

20. B. Nilsson, "Metorological Influence on Aerosol Extinction in the 0.2 - 40μm Wavelength Range," Appl. Opt. 18, 3457 (1979).

REFERENCES

1. E. R. Murray and J. E. van der Laan, "Remote Measurement of Ethylene Using a CO_2 Differential-Absorption LIDAR", Appl. Opt. 17, 814 (1978).
2. D. K. Killinger and N. Menyuk, "Remote Probing of the Atmosphere Using a CO_2 DIAL System", IEEE J. Quantum Electron. QE-17, 1917 (1981).
3. N. Menyuk, D. K. Killinger and W. E. DeFeo, "Remote Sensing of NO Using a Differential Absorption LIDAR", Appl. Opt. 19, 3282 (1980).
4. R. A. Baumgartner and R. L. Byer, "Remote SO_2 Measurements at 4μm with a Continuously Tunable Source", Opt. Lett. 2, 163 (1978).
5. K. Asai, T. Itabe and T. Igarashi, "Range Resolved Measurements of Atmsopheric Ozone Using a Differential-Absorption CO_2 Laser Radar", Appl. Phys. Lett. 35, 60 (1979).
6. R. C. Harriss and J. T. Michaels, "Sources of Atmospheric Ammonia", Second Symposium, Composition of the Nonurban Troposphere (1982).
7. R. Abbas and R. L. Tanner, "Continuous Determination of Gaseous Ammonia in the Ambient Atmosphere Using Fluorescence Derivatization", Atmos. Environ. 15, 277 (1981).
8. N. C. Lau and R. J. Charlson, "Discrepancy Between Background Atmospheric Ammonia Gas Measurement and Existence of Acid Sulfate as a Dominant Atmospheric Aerosol", Atmos. Environ. 11, 475 (1977).
9. N. Menyuk and D. K. Killinger, "Temporal Correlation Measurements of Pulsed Dual CO_2 LIDAR Returns," Opt. Lett. 6, 301 (1981).
10. N. Menyuk and D. K. Killinger, "Assessment of Relative Error Sources in IR DIAL Measurement Accuracy", Appl. Opt. 22, 2690 (1983).
11. N. Menyuk and P. F. Moulton, "Development of a High-Repetition-Rate Mini-TEA CO_2 Laser", Rev. Sci. Instrum. 51, 216 (1980).

Ambient concentrations varying between zero and 20 ppb were measured in real time, and the system was shown to be capable of detecting atmsopheric NH_3 concentration variations of a few parts per billion, in reasonable agreement with the calculated sensitivity.

The concentration of ambient NH_3 was found to be negatively correlated with the relative humidity. This was shown to be consistent with the changes that are known to take place in atmospheric aerosols with changes in relative humidity.[19,20] At humidities above 50% the NH_3 is washed from the air by the wet particles, but as the relative humidity drops below about 50% NH_3 is released by the aerosols. While the experimental data is consistent with this hypothesis, further studies will be required in order to further document the effect.

NH_3 is extremely soluble in water (251.6 g/ℓ) and is rapidly removed from the atmosphere by aqueous aerosols, which provides a reasonable explanation for the observed NH_3 change in Fig. 5. . Aerosol particle growth is a function not of the quantity of precipitable water in the air but of the relative humidity, being slight for relative humidities less than 50% and increasing rapidly with increasing relative humidity.[19] This aerosol growth factor may also be correlated to the fact that the solubility of gaseous ions onto the surface of atmospheric aerosols has been shown to depend significantly upon a Critical Relative Humidity (CRH), being very low for values less than the CRH, and extremely soluble for large values.[20] Small changes in the relative humidity around this critical value can result in a very large change in the concentration of the gaseous species. Typical CRH values range in the order of 50 to 70% for several ionic species in aqueous solution including NH_4NO_3 and NH_4Cl. While the CRH value for NH_3 (i.e., NH_4OH in solution) is not directly known, it is anticipated that a similar value would apply. If this is the case, a reasonable explanation for the data observed in Fig. 5 is that for a relative humidity of 54%, the aerosol particles are essentially wet and have absorbed most of the soluble NH_3 gas from the air; when the relative humidity drops to 41%, the aerosol particles act as dry particles releasing the absorbed NH_3. Obviously, much further expermental work will be required in order to determine the validity of this assertion as well as the underlying rate constants.

VI. Conclusions

A CO_2 laser DIAL system has been used to remotely detect the path-averaged concentration of NH_3 in the atmosphere over a range of 2.7 km.

produced data that varied by only about 10% in the determination of Pa/Pa' in Eq. (1); this factor corresponds to an uncertainly in the determination of the NH_3 concentration of about 3 ppb.

The resultant DIAL data are given in Fig. 4 and show a path-averaged NH_3 concentration of 15 ± 5 ppb over a period of about one hour; these measurements were made when the relative humidity was about 26%. As seen in the data, the overall accuracy of the DIAL measurement is better than that shown in Fig. 3 due to the use of the stronger absorption line, R(30).

The single-laser DIAL experiments were repeated on another day; in this case, however, the relative humidity was initially 54% (temperature approximately 50 ^{o}F) and there was a considerable amount of haze. The data are given in Fig. 5 and indicate essentially zero NH_3 concentration present in the atmosphere during the morning hours when the humidity was high. Early in the afternoon the haze burned off and there was a drop in humidity to 41% (temperature approximately 60^{o}F). With this change in humidity, NH_3 concentration rose to 20 ± 5 ppb. This negative correlation between relative humidity and measured NH_3 concentration was also observed on several other days with similar meteorological behavior. This observed NH_3 and humidity anti-correlation is not believed to be caused by changes in the concentration of water vapor leading to a water vapor induced differential-absorption signal. In this regard, it is estimated that the absolute water vapor concentration varied by 8% from 5.0 Torr (54% relative humidity, 50^{o}F) to 5.4 Torr (41% relative humidity, 60^{o}F). Using this variation in the (α - α') term in Eq. (1), one estimates that such a change would only influence the deduced concentration of NH_3 by 0.3 ppb, a value negligible in comparison to the observed NH_3 change.

very low output energy (< 0.5 mJ/pulse) of the CO_2 laser on the R(30) or R(26) line. Details of these two experiments follow.

In the first experiment Laser 1 was tuned to the P(30) reference line and Laser 2 was tuned to the P(32) line near 9.7 μm. The LIDAR returns from the two lasers were collected and averaged for 500 pulses (30 seconds). The deduced path-averaged NH_3 concentration is plotted against the time of day in Fig. 3. Peaks of 10 to 20 ppb were occasionally observed above a baseline scatter of 10 ppb; this includes an estimated bias of 8 ppb due to the $(\alpha - \alpha')$ term in Eq. (1). While the observed peaks are not much higher than the estimated background, the data is suggestive that the observed DIAL signal is due to atmospheric NH_3, and not an artifact, since other atmospheric species which absorb radiation at the P(32) laser line, such as $CHCl_3$ and CF_2Cl_2, also have similar absorbance at the P(30) line.[17] In addition, the 10 to 20 ppb of NH_3 observed is in good agreement with the 2 to 20 ppb that is considered to be normal in the atmosphere.[18]

Measurements using the more optimal R(30) and R(26) lines near 9.2μm band were attempted to take advantage of greater sensitivity available at these frequencies. Because the CO_2 laser energy was limited to about 0.5 mJ on the R(30) or R(26) line, the returns from a diffuse target at a range of 2.7 km produced a signal-to-noise ratio of less than one. To increase the signal-to-noise ratio, the LIDAR was directed to a one-inch retroreflector at the same range. Although this gave a stronger return, the small target size and the deflection of the beam by atmospheric turbulence increased the standard deviation of the individual returns. However, signal averaging over 500 pulses

Initial DIAL calibration measurements of NH_3 were made using the polypropylene tank shown in Fig. 1. The tank was purged with dry N_2 for one hour and placed in the LIDAR path. The 100% transmittance baselines for the P(30) and P(32) lines were obtained by averaging the normalized LIDAR returns from a building at a range of 2.7 km for 1000 pulses. A 0.2 cm^3 sample of 28% aqueous NH_3 was then injected into the tank. The change in the LIDAR returns as the NH_3 solution evaporated in the tank is shown in Fig. 2.

As seen in Fig. 2, the transmittance values of the P(30) and P(32) lines, after a steady state was reached, were 0.81 and 0.12, respectively. The concentration of NH_3 in the tank was estimated to be 220 ppm; the 0.2 cm^3 sample of 28% NH_3 with a specific gravity of 0.898 g/cm^3 yields 1.8×10^{21} molecules of NH_3 in the 319 liter tank. With these transmission values, NH_3 concentration levels, and a round-trip path length through the cell of 208 cm, the experimental absorption coefficients for the P(30) and P(32) lines were 1.1 $(atm\ cm)^{-1}$ and 12 $(atm\ cm)^{-1}$, respectively. These values are in good agreement with those measured in the laboratory absorption cell and the data given in Table I.

V. Laser Remote Sensing of Atmospheric NH_3

The DIAL system was used to detect and measure the path-averaged concentration of ambient atmospheric NH_3. Two different experiments were performed. The first experiment involved the use of the dual-laser DIAL system; these measurements used the less than optimal P(30) and P(32) CO_2 laser lines and LIDAR returns from topographic targets. The second set of experiments used a single-laser DIAL system; these measurements employed the more optimal R(30) and R(26) lines, but used LIDAR returns from a retroreflector due to the

McClatchey et al.[14] As seen in Table I, significant absorption by NH_3 occurs in both the 10.6 μm and 9.6 μm transition bands of the CO_2 laser. The most suitable laser transition pair seems to be the R(30) transition at 9.217 μm as the high-absorption line and the R(26) transition at 9.237 μm as the low-absorption line. However, only one CO_2 laser could be made to operate on these two lines, so that only a single-laser DIAL experiment was possible using these "optimal" lines. Dual-laser DIAL experiments were carried out using the less optimal P(32) transition at 10.716 μm as the high-absorption line and the P(30) transition at 10.693 μm as the low-absorption line. These two line pairs provide closely spaced frequencies, which helps to maximize the mutual coherence[15] of the two laser beams. It should be noted that while a dual-laser DIAL measurement may be more accurate in the determination of (P_a/P_a') by a factor of as much as 2 or 3 over that of a single-laser DIAL measurement,[2] this factor can be more than compensated in Eq. (1) by the increased accuracy due to the use of an "optimal" absorption line where $(\sigma_a' - \sigma_a)$ is large; such is the case for the two line pairs for NH_3 detection presented in this paper.

IV. Ammonia Absorption Measurements and Calibration

The absorption coefficients of NH_3 were measured using the laboratory absorption cell shown in Fig. 1. The CO_2 lasers were tuned to the appropriate transitions and the normalized intensities of the laser beams after passage through the cell were detected and averaged for 1000 pulses. The cell was filled with a mixture of 780 ppm NH_3 in air. The transmittance values obtained correspond to an absorption coefficient, σ, of 60 $(\text{atm cm})^{-1}$ and 13 $(\text{atm cm})^{-1}$ for the two high-absorption R(30) and P(32) transitions, respectively. These results are in good agreement with those shown in Table I and the recent NH_3 absorption data of Hawley, et al.[16]

those laser transitions available from the CO_2 lasers used. Secondly, the difference in the absorption levels of the two laser frequencies used in a DIAL measurement must be sufficient to yield a meaningful differential absorption in the LIDAR returns for accurate atmospheric remote-sensing measurements. In addition, atmospheric transmission and possible interference effects from other atmospheric species must be considered.

The trade-off of these factors may be seen in Eq. (1), which gives the deduced path-averaged concentration of the absorbing molecule, N_a, over the range, R, as

$$N_a = \ell n\,(P_a/P_a') + 2\,(\alpha - \alpha')R \;/\; 2(\sigma_a' - \sigma_a)\,R \quad , \qquad (1)$$

where P_a is the backscattered signal power normalized to the transmitted power, σ_a is the molecular absorption cross section, and α is the background extinction coefficient of the atmosphere; the primed and unprimed parameters refer to values at the low- and high-absorption frequencies, respectively.[10] As seen in Eq. (1), the accuracy in the measurement of N_a is increased when $(\sigma_a' - \sigma_a)$ is large, the accuracy in the measurement of P_a/P_a' is high, and $(\alpha - \alpha')$ is negligible.

Based upon the above criteria, possible laser lines for the remote sensing of NH_3 along with the corresponding absorption coefficients of NH_3 and the atmospheric extinction are given in Table I. The NH_3 absorption coefficients for these CO_2 laser lines[11] were obtained from measurements by Patty et al.[12] and by Brewer and Bruce.[13] The atmospheric transmission and possible interference from other molecules were obtained from the AFGL tapes of

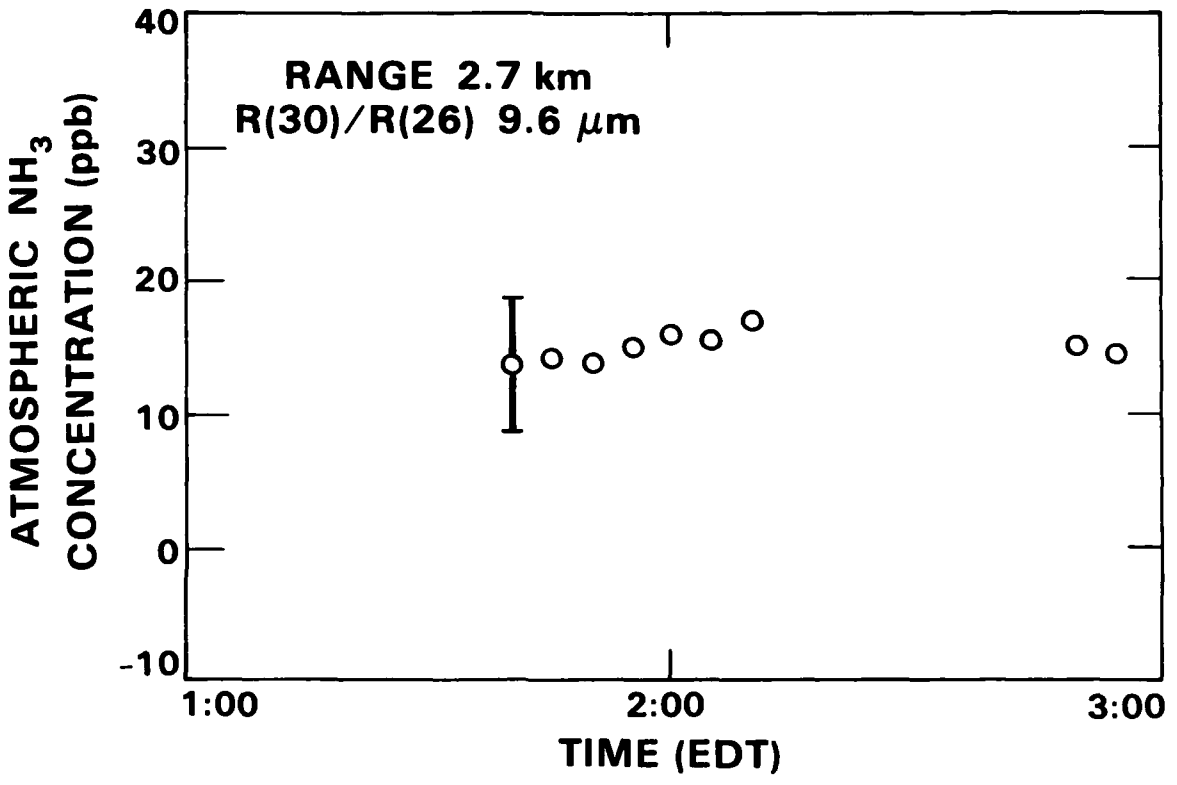

129637-N

Figure 4.

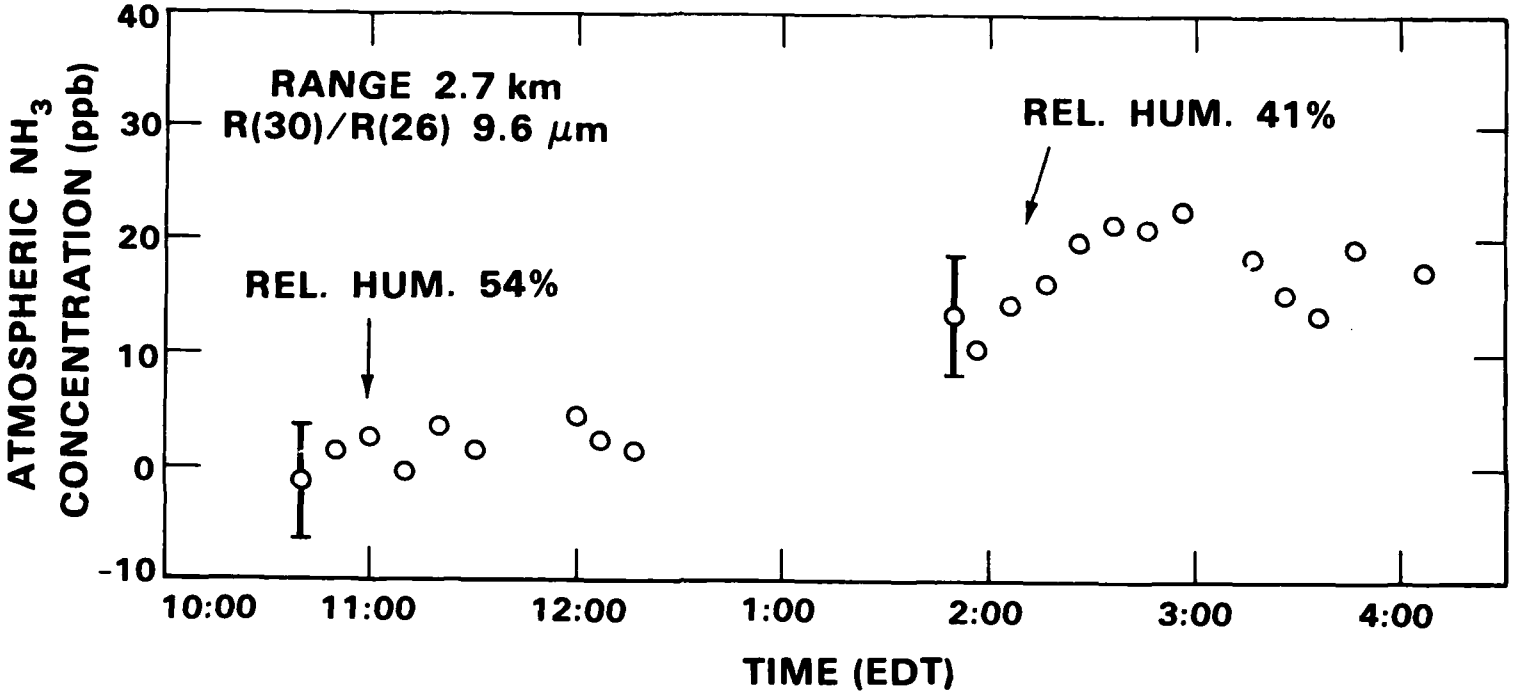

Figure 5.

129635-N

UNCLASSIFIED

SECURITY CLASSIFICATION OF THIS PAGE *(When Data Entered)*

A159531

REPORT DOCUMENTATION PAGE		READ INSTRUCTIONS BEFORE COMPLETING FORM
1. REPORT NUMBER ESD-TR-85-212 ESL-TR-85-34	2. GOVT ACCESSION NO.	3. RECIPIENT'S CATALOG NUMBER
4. TITLE *(and Subtitle)* Laser Remote Sensing of Atmospheric Pollutants		5. TYPE OF REPORT & PERIOD COVERED Final Report 1 October 1983 — 30 September 1984
		6. PERFORMING ORG. REPORT NUMBER
7. AUTHOR(s) Dennis K. Killinger, Norman Menyuk, Aram Mooradian		8. CONTRACT OR GRANT NUMBER(s) F19628-85-C-0002
9. PERFORMING ORGANIZATION NAME AND ADDRESS Lincoln Laboratory, M.I.T. P.O. Box 73 Lexington, MA 02173-0073		10. PROGRAM ELEMENT, PROJECT, TASK AREA & WORK UNIT NUMBERS Program Element Nos.63723F and 63745F Project No.1900
11. CONTROLLING OFFICE NAME AND ADDRESS Engineering and Services Laboratory Air Force Engineering and Services Center Tyndall AFB, FL 32403		12. REPORT DATE 30 September 1984
		13. NUMBER OF PAGES 60
14. MONITORING AGENCY NAME & ADDRESS *(if different from Controlling Office)* Electronic Systems Division Hanscom AFB, MA 01731		15. SECURITY CLASS. *(of this Report)* Unclassified
		15a. DECLASSIFICATION DOWNGRADING SCHEDULE

16. DISTRIBUTION STATEMENT *(of this Report)*

Approved for public release; distribution unlimited.

17. DISTRIBUTION STATEMENT *(of the abstract entered in Block 20, if different from Report)*

18. SUPPLEMENTARY NOTES

None

19. KEY WORDS *(Continue on reverse side if necessary and identify by block number)*

laser remote sensing,
environmental monitoring,
differential absorption LIDAR (DIAL),
CO_2 and Co:MgF_2 DIAL systems
ammonia, hydrogen chloride,

20. ABSTRACT *(Continue on reverse side if necessary and identify by block number)*

The specific tasks carried out during FY84 for this research program consisted of the following: (1) Continuation of the CO_2 DIAL program with a remote sensing measurement of NH_3 and an analysis of system accuracy limitations, (2) further improvements in the Co:MgF_2 DIAL system measurement capability, (3) column-content remote sensing of HCl and initial range-resolved H_2O concentration measurements with the Co:MgF_2 DIAL system, and (4) initial investigation of frequency shifting the Co:MgF_2 laser radiation.

Originator Supplied Keywords Included:

DD FORM 1 Jan 73 1473 EDITION OF 1 NOV 65 IS OBSOLETE

UNCLASSIFIED

SECURITY CLASSIFICATION OF THIS PAGE *(When Data Entered)*

END

FILMED

11-85

DTIC